Modeling the impediment of methane ebullition bubbles by seasonal lake ice

S. Greene[a], K. M. Walter Anthony[b*], D. Archer[c], A. Sepulveda-Jauregui[b], K. Martinez-Cruz[b,d]

[a] Department of Chemistry, The University of Chicago, Chicago, Illinois, USA

[b] Water and Environmental Research Center, Institute of Northern Engineering, University of Alaska-Fairbanks, Fairbanks, Alaska, USA

[c] Department of the Geophysical Sciences, The University of Chicago, Chicago, Illinois, USA

[d] Biotechnology and Bioengineering Department, Cinvestav, Mexico City, D. F., Mexico

[*]Corresponding author: kmwalteranthony@alaska.edu

Abstract

Microbial methane (CH_4) ebullition (bubbling) from anoxic lake sediments comprises a globally significant flux to the atmosphere, but ebullition bubbles in temperate and polar lakes can be trapped by winter ice cover and later released during spring thaw. This "ice-bubble storage" (IBS) constitutes a novel mode of CH_4 emission. Before bubbles are encapsulated by downward-growing ice, some of their CH_4 dissolves into the lake water, where it may be subject to oxidation. We present field characterization and a model of the annual CH_4 cycle in Goldstream Lake, a thermokarst (thaw) lake in interior Alaska. We find that summertime ebullition dominates annual CH_4 emissions to the atmosphere. Eighty percent of CH_4 in bubbles trapped by ice dissolves into the lake water column in winter, and about half of that is oxidized. The ice growth rate and the magnitude of the CH_4 ebullition flux are important controlling factors of bubble dissolution. Seven percent of annual ebullition CH_4 is trapped as IBS and later emitted as ice melts. In a future warmer climate, there will likely be less seasonal ice cover, less IBS, less CH_4 dissolution from trapped bubbles, and greater CH_4 emissions from northern lakes.

1 Introduction

Globally, the magnitude of methane (CH_4) emissions from freshwater lakes (72 Tg CH_4 yr^{-1}; Bastviken et al., 2011) constitutes an estimated 30% of all natural emissions (217 Tg CH_4 yr^{-1}; IPCC, 2013). Methane is typically produced in anoxic bottom sediments by methanogenic microbes and can be released to the atmosphere by diffusion, vascular transport through aquatic plants, or ebullition (bubbling) (Rudd and Hamilton, 1978; Bastviken et al., 2004; Whalen, 2005). Methanogenesis in the oxic water column has been proposed as an additional CH_4 source in some lakes (Tang et al., 2014). In many lakes, ebullition from bottom sediments is the dominant mode of emission because gas-phase CH_4 in bubbles is not subject to oxidation, whereas a significant proportion of dissolved CH_4 is typically oxidized by methanotrophic bacteria, including in the plant rhyzosphere (Keller and Stallard, 1994; Casper et al., 2000; Bastviken et al., 2008).

Most ebullition CH_4 in shallow lakes is released directly to the atmosphere in the summer, but in cold-climate regions bubbles are trapped beneath and encapsulated by downward-growing lake ice in the winter (Walter et al., 2006). Methane involved in this "ice-bubble storage" (IBS) is later released during spring thaw. The CH_4 content of bubbles decreases as they are encapsulated, which suggests CH_4 dissolution into the water column (Walter et al., 2008). Dissolved CH_4 accumulates in many lakes during the ice cover period due to the slowdown or inactivity of methanotrophs in the cold, often anoxic water column (Michmerhuizen et al., 1996; Phelps et al., 1998; Boereboom et al., 2012), so dissolved CH_4 from bubbles may not be immediately subject to oxidation. However, it can potentially be oxidized when oxygen is reintroduced during spring ice melt. The fraction of CH_4 that escapes to the atmosphere from seasonally ice-covered lakes depends on these biogeochemical processes.

Previously, Sasaki et al. (2009) measured the CH_4 concentration of bubbles trapped within lake ice in Antarctica and used aerial imaging to estimate the total volume of gas trapped before the ice melts. Elsewhere, others have measured dissolved CH_4 concentrations beneath winter lake ice or the CH_4 diffusion rate following ice-off to estimate net springtime emissions (e.g., Michmerhuizen et al., 1996; Phelps et al., 1998; Smith and Lewis, 1992).

In North Siberian thermokarst (thaw) lakes, ebullition occurs mainly at discrete locations ("seeps") on the lake bottom (Walter et al., 2006). Bubbles trapped within the ice above seeps (at "seep sites") are easily visible in early-winter lake ice (Fig. 1a). Walter et al. (2006) defined four classes of seeps: A, B, C, and Hotspot (Fig. 1b). A-type seeps exhibit lower ebullition rates and a greater degree of separation among ice-trapped bubbles; B- and C-type seeps exhibit progressively higher ebullition rates and greater degrees of bubble coalescence in ice. Ebullition rates are highest for Hotspots, where frequent bubbling brings warmer water from the lake bottom to the surface, maintaining open water during a portion of the ice-cover period. When air temperatures are sufficiently cold, a thin layer of ice covers Hotspot seep sites, beneath which gas accumulates in a cavity open to the water column. Using submerged bubble traps placed above seeps to measure short- and long-term (year-round) seep-class ebullition rates and counts of ebullition seep sites in lake-ice transects, Walter Anthony and Anthony (2013) estimated whole-lake seep ebullition. Translating seep ebullition to atmospheric CH_4 emission from seeps was not possible due to a lack of knowledge about the degree to which seasonal lake ice reduces ebullition emissions.

This manuscript describes the formulation of a model, informed by field measurements, of CH_4 dissolution from trapped ebullition bubbles in Goldstream Lake, a thermokarst lake in interior Alaska. This study has three goals: (1) to gain insight into how some physical and

biogeochemical processes within a thermokarst lake interact to determine seasonal and annual CH_4 emissions via diffusion, ebullition, and IBS, (2) to determine the extent to which lake ice reduces net annual emissions, and (3) to gain insight into how changes in climate will influence emissions by different modes in the future.

2 Methods

2.1 Study site

Goldstream Lake (informal name; 64.92˚ N, 147.85˚ W; area 10,030 m^2; volume 15,700 m^3; mean depth 1.6 m; max. depth 2.9 m) is located near the bottom of Goldstream Valley in the discontinuous permafrost zone of interior Alaska. The lake formed by the melting of permafrost ground ice in retransported late-Quaternary loess common on many hill slopes and valley bottoms of interior Alaska (Muhs and Budahn, 2006). Colluvial forces and frost action gradually eroded loess downslope during the late Pleistocene and early Holocene, forming icy, organic-rich deposits known as "yedoma" frequently several tens of meters deep in valley bottoms (Péwé, 1975; Muhs and Budahn, 2006; Reyes et al., 2010; Kanevskiy et al., 2011). Ice wedges 2 to 4 m wide at their tops and up to tens of meters deep are common in this type of permafrost (Hamilton et al., 1988). Ground-ice melt leads to collapse of the surface and ground subsidence, a process known as thermokarst (Mackay, 1970). Ponding of water in depressions further accelerates permafrost thaw, leading to expansion and deepening of thermokarst lakes over time. Remote-sensing observations of Goldstream L. showed that a partial drainage event occurred in the lake sometime after 1949; however, thermokarst expansion continues today, predominantly along its eastern margin (the "thermokarst zone," Fig. 2). Walter Anthony and Anthony (2013) observed

higher ebullition activity within this zone (i.e., a greater density of seeps, particularly high-flux Hotspot seeps) than in the remainder of the lake (the "non-thermokarst zone").

2.2 Field observations

2.2.1 Lake bathymetry

During the winter of 2011–2012, we mapped the bathymetry of Goldstream L. using sonar point measurements (Vexilar LPS-1 Hand-Held Depth Finder, Minneapolis, Minnesota, USA) through ice or in ice-augered holes combined with centimeter-accuracy RTK differential GPS (Leica Geosystems AG, Heerbrugg, Switzerland) at 99 distributed locations on the lake. In late October 2011, depth measurements were obtained using sonar through ice at 347 points within two rectangular plots in the lake center and northeast thermokarst zone at a density of approximately 0.22 measurements per m^2. We produced an interpolated bathymetric map using kriging in ArcGIS (Esri, Redlands, California, USA). The resulting map was used to create a three-dimensional model of the lake in ArcScene (Esri), from which we estimated the water volume in 0.5 m depth intervals relative to the water level on 30 October 2011, the date of > 95% of bathymetry measurements.

2.2.2 Water level

Measurements of hydrostatic pressure at the bottom of Goldstream L. (Global Water WL 16 vented submersible pressure transducer with a Global Logger v2.1.4 data logger, College Station, Texas, USA) were used to estimate changes in the lake's water level and volume throughout the study period. We define the water level during the ice-cover period as the height of the water column at the measurement site if, hypothetically, all of the snow and ice on the lake surface melted. Hydrostatic pressure measurements were not available from 21 May 2011 to 14 February 2012 and on several dates in the fall of 2012. From 12 October 2011 to 14 February

2012, we used daily precipitation measurements (Sect. 2.2.8) to extrapolate the water level backward from 14 February 2012. The water level from 21 May 2011 to 11 October 2011 and on dates in the fall of 2012 was linearly interpolated between adjacent values (Fig. B1).

2.2.3 Water temperature

Temperature-depth profiles were obtained within Goldstream L. between 19 October 2010 and 2 July 2012 using a handheld Hach DS5 Multiprobe Sonde (Hach Hydromet, Loveland, Colorado, USA). Measurements were obtained at approximately 5 depths at each of two sites on each sampling day. Additionally, we measured water column temperatures at depth intervals of 0.5 m from the lake surface hourly from 10 April 2009 through 8 December 2013 using Hobo Water Temperature/Light pendant loggers (Onset, Bourne, Massachusetts, USA). One logger was located near the center of Goldstream L. and another in the thermokarst zone.

2.2.4 Lake ice types and phenology

Congelation (black) ice is formed when water freezes at the bottom of the ice layer and therefore appears clear. In contrast, snow (white) ice is opaque and is formed when the weight of snow depresses the ice surface beneath the water level, causing lake water to flood snow on top of the ice layer and freeze. During the ice-cover seasons from October 2010 to May 2012, we obtained the thicknesses of each type of ice, as well as that of snow, by augering a hole in the ice (20 cm diameter) near the lake center, measuring the total ice and snow thicknesses around the auger hole, and looking through the hole for differences in ice color to estimate white and black ice thicknesses with a measuring tape. In the winter of 2010–2011, measurements were made where snow was occasionally compacted by foot traffic; measurements in 2011–2012 were made in undisturbed locations. Using a time-lapse camera (Game Spy I-60, Moultrie, Alabaster, Alabama, USA) we acquired images of the lake surface every four hours from 16 April 2010 to

14 May 2010 to constrain the timing of freeze-up and ice-off (the first and last days of any observed ice cover, respectively).

2.2.5 Water column dissolved gases

Dissolved CH_4 concentration-depth profiles were measured in the center of Goldstream L. and 5 m away from the eastern shore on 34 days between 27 October 2010 and 22 September 2012. Duplicate water samples were collected from a boat in summer or from the lake ice surface through an auger hole in winter. Water samples (10 mL) collected with a Van Dorn bottle (Wildco, Yulee, Florida, USA) were gently transferred into 25 mL glass serum bottles and immediately sealed with butyl rubber stoppers and aluminum crimp caps. Bottles were stored upside down and frozen in the dark until laboratory analysis. We thawed samples overnight in the refrigerator, brought them to room temperature for 10 minutes, and shook them for 15 seconds to equilibrate headspace and water. We then measured the CH_4 concentration in the headspace using a GC-2014 gas chromatograph (Shimadzu, Addison, Illinois, USA) equipped with a flame ionization detector and a PLOT alumina column (detector temperature 250 °C, oven 40 °C, high purity Helium as carrier gas). Dissolved CH_4 concentrations were calculated from headspace CH_4 concentrations using a temperature-dependent Henry's Law constant (Wilhelm et al., 1977).

Dissolved oxygen (O_2) concentrations were measured simultaneously with water temperature using a Clark-type microelectrode on the calibrated Hach DS5 Multiprobe Sonde (Sect. 2.2.3).

Measured concentrations were used to estimate total amounts of CH_4 and O_2 dissolved in Goldstream L. To facilitate comparison with our model, interpolated concentration profiles were integrated with respect to depth using bathymetry measurements to calculate total quantities of

152 dissolved gas separately in the upper 1.25 m of the water column and in the lower layer (below
153 1.25 m). The volume of the upper layer was adjusted to account for changes in the ice/snow layer
154 thickness, calculated using our ice growth model (Sect. 2.3.2).

155 **2.2.6 Ebullition**

156 Seep ebullition in Goldstream L. was characterized using methods described previously
157 by Walter Anthony et al. (2010). We used average areal densities (seeps m^{-2}) for each class
158 measured by Walter Anthony and Anthony (2013) in transects covering 11% of Goldstream L.,
159 plus another, subsequent 428 m^2 survey plot that increased the total area of the lake surveyed for
160 A, B and C-type seeps to 15%. The entire lake surface was surveyed for Hotspot seeps. The
161 resulting seep densities (A, 0.31 seeps m^{-2}; B, 0.08 seeps m^{-2}; C, 0.03 seeps m^{-2}; and Hotspot,
162 0.01 seeps m^{-2}) were used as inputs to the model.

163 Seep class-specific smoothed ebullition rates (mL gas $seep^{-1}$ d^{-1}), indexed by Julian Day,
164 were applied to all seeps in the model. These were calculated from long-term (up to 700 days)
165 measurements of daily ebullition rates for 31 seeps in four Arctic thermokarst lakes (Walter
166 Anthony et al., 2010). Twelve of these seeps were located in Goldstream L., and average
167 bubbling rates for each class of seeps in Goldstream L. were not significantly different from the
168 Arctic averages. We calculated the mean ebullition rate on each Julian Day for each class from
169 our measurements of individual seeps. Because ebullition from individual seeps is often highly
170 episodic, and because there were significant data collection gaps for many seeps, resulting in
171 certain Julian Days on which only a few seeps were represented in the average, the resulting
172 annual flux cycle represented by Julian Day averages was highly irregular. We smoothed Julian
173 Day averages three times by taking 30-day running averages of daily averages in order to remove
174 these irregularities, as we wanted this smoothed data to represent the annual ebullition cycle

175 rather than the ebullition dynamics of individual seeps. This smoothing did not change the total
176 calculated yearly amount of CH_4 released from seeps by ebullition.

177 For comparison with smoothed fluxes in a sensitivity analysis of the model, we also used
178 measured fluxes from individual seeps with relatively few data gaps, which were scaled and
179 applied to the 2010–2012 study period. In the sensitivity analysis, we included measurements of
180 nine A-type seeps, seven B-type seeps, five C-type seeps, and seven Hotspots in Goldstream L.,
181 Cranberry Lake (interior Alaska), Shuchi Lake (Siberia), and Grass Lake (Siberia) year-round
182 during one or more years between 2003 and 2014. All of these lakes are thermokarst lakes that
183 formed in yedoma-type permafrost deposits. Smoothed and individual seep fluxes are presented
184 in Fig. 3.

185 During the period of decreasing ice thickness in the spring (the "ice-melt period"), when
186 standing water was present on the ice surface, we observed gas escaping from bubbles trapped by
187 the ice. On 18 April 2010 and 21 April 2011, we collected such gas from eight ice-trapped
188 bubbles in Goldstream L., four of which were located above the same ebullition seep. Gas was
189 collected by displacement into inverted, water-filled glass serum bottles, which were then sealed
190 with butyl rubber stoppers and aluminum crimp caps until later analysis. Additionally, bubbles
191 from 246 ebullition events in Goldstream L. were collected from submerged bubble traps above
192 ebullition seeps from 2008 to 2011 following methods described by Walter et al. (2008). These
193 "fresh" samples enabled us to calculate the CH_4 composition of bubbles after they ascend
194 through the water column but before they interact with lake ice, allowing for the conversion of
195 measured volumetric fluxes (ml gas $seep^{-1}$ d^{-1}) to molar fluxes (mol CH_4 $seep^{-1}$ d^{-1}). All samples
196 were transported to the lab and stored under refrigeration, in the dark. The CH_4 concentrations of
197 samples were analyzed using the Shimadzu GC-2014 gas chromatograph.

198 Additionally, blocks of ice were harvested from ebullition seep sites with a chainsaw in
199 the late winter and early spring, and the shapes of encapsulated bubbles and cavities within ice
200 blocks were measured (Fig. 1c).

201 **2.2.7 Ice-bubble mesocosms**

202 Measurements of the rate of CH_4 diffusion from submerged, gas-filled mesocosm
203 chambers constrained our model of diffusion from trapped bubbles. During each of two trials
204 (spring and fall, 19–24 April 2011 and 30 October – 6 November 2011), we suspended 24
205 chambers approximately 14 cm below the water surface in random positions within two 1 m by 3
206 m holes opened in the ice near the center of Goldstream L. The observation of relatively few ice-
207 trapped bubbles in bubble transect surveys in the lake's center suggests that rates of natural
208 ebullition from the sediments are relatively low there. Mesocosm chambers consisted of inverted
209 containers (14 cm by 14 cm by 25 cm tall; Tupperware, Orlando, Florida, USA) filled with lake
210 water and fitted with a three-way stopcock to release gas. A gas standard (140 mL) with a
211 composition similar to that of natural seep ebullition bubbles (80% CH_4, 20% N_2) was then
212 injected such that its height within each chamber (approx. 10 mm) approximated the measured
213 thickness of small bubbles trapped beneath ice (5.7 ± 1.0 mm, mean ± standard deviation).
214 Chambers were open to lake water but fitted with deflectors beneath to deter natural ebullition
215 bubbles from entering. At 1-day intervals (including a time zero control), we recovered gas from
216 triplicate chambers and measured its volume and CH_4 composition. Re-growth of lake ice above
217 the chambers did not reach 14 cm, so no chambers became surrounded by ice.

218 The following equation, which is based on Fick's First Law in one dimension, gives the
219 CH_4 dissolution flux, J, from chambers (Holocher et al., 2003):

220 $$J = D_{CH4} \frac{[CH_4]_{eq} - [CH_4]}{\delta_{eff}} \quad (1)$$

where D_{CH4} is the diffusivity of CH_4 in water (0.98×10^{-9} m^2 s^{-1}; Broecker and Peng, 1974), and $[CH_4]_{eq}$ and $[CH_4]$ are the equilibrium and bulk concentrations of dissolved CH_4 in lake water. δ_{eff} represents an effective diffusively controlled layer thickness, calibrated such that the gradient calculated from $[CH_4]_{eq}$, $[CH_4]$, and δ_{eff} equals the true gradient at the bubble's surface. The CH_4 mole fraction determines $[CH_4]_{eq}$, based on the hydrostatic pressure in the chamber and a Henry's Law constant of 2.533×10^{-5} mol L^{-1} kPa^{-1} for CH_4 in water at 0 ˚C (Yamamoto et al., 1976). The bulk CH_4 concentration was taken to be the average concentration in the upper 1.25 m of the water column, calculated from measurements (Sect. 2.2.5).

A simple model based on Eq. (1) with a 1-hour time step was used to simulate CH_4 dissolution from chambers. For each trial, δ_{eff} was calibrated to optimize the fit between the modeled and measured CH_4 composition and volume. The exchange of other gases between chambers and the water column was neglected, as we estimated that including N_2 exchange has a negligible (approx. 7%) effect on the magnitude of CH_4 dissolution. This model exhibited close fits to measurements at the optimum values of δ_{eff} (0.25 mm and 0.27 mm for the spring and fall trials, respectively, Fig. 4). Because δ_{eff} values were fairly consistent between trials, which were conducted in conditions with substantially different upper-layer CH_4 concentrations (290 and 2 μM in spring and fall trials, respectively), we applied this formula with a δ_{eff} of 0.26 mm in our model of CH_4 diffusion from trapped ebullition bubbles (Sect. 2.3.3).

2.2.8 Meteorological observations

Daily measurements of maximum and minimum air temperature, barometric pressure, precipitation, wind velocity, and snow depth were obtained from a U. S. National Weather Service Co-Op site located approximately 2.6 km southwest of Goldstream L. Minimum and maximum temperatures were averaged to calculate daily mean temperatures.

2.2.9 Atmospheric CH_4 concentrations

We monitored the concentration of atmospheric CH_4 50 cm above the lake surface from 12 April 2010 to 9 May 2011 using a LI-7700 Open Path Methane Analyzer (LI-COR Biosciences, Lincoln, Nebraska, USA) mounted on a stationary raft. The radius of its concentration measurement footprint was approximately 60 m (area 10,600 m^2; Gash, 1986). The lake surface occupied the majority of the footprint; however, littoral vegetation and black spruce forest-tundra occupied approximately 30% of the footprint, primarily in the southeastern quadrant (Fig. 2). The prevailing wind direction in Goldstream Valley from 2008 to 2013 was from the N in summer and from the NNE the remainder of the year; thus the terrestrial contribution to the LI-7700 signal should have been minimal. Measurements of atmospheric CH_4 concentration were obtained five times per second and converted to daily averages.

2.2.10 Methane diffusion from sediments

We calculated the rate of CH_4 diffusion into the water column from CH_4-rich lake bottom sediments using measurements of CH_4 concentrations in the surface sediments of Vault Lake, a thermokarst lake near Goldstream L., because measurements from Goldstream L. were unavailable. Since Vault L. formed in similar yedoma-type permafrost deposits, we assumed that sediment concentrations from Vault L. were representative of Goldstream L. We obtained two sediment cores in March 2013 from a location in between the center and active thermokarst margin of Vault L. and kept the cores under refrigeration at 2 ˚C prior to laboratory analysis. Triplicate samples (5 mL each) were obtained with a syringe at multiple depths within the top 5 cm of the cores and transferred to 20 mL serum vials containing 10 mL of water. Vials were sealed with rubber caps. The CH_4 concentration in the water was determined using methods described previously in Sect. 2.2.5 and converted to a CH_4 concentration per unit sediment

267 volume. This was converted to a concentration per unit water volume using measurements of
268 sediment density in Vault L. (K. M. W. A., unpublished data). The resulting concentration
269 gradient between the topmost two measurements was multiplied by the molecular diffusivity of
270 CH_4 to calculate the diffusive flux according to Fick's First Law.

271 The methanogenic rate in the sediments of Goldstream L. varies with temperature
272 throughout the year (Schulz et al., 1997; Sepulveda-Jauregui et al., 2014a). In order to quantify
273 this effect on sediment diffusion rates in the model, we monitored the temperature of surface
274 sediments in Goldstream L. from 3 July 2008 to 23 March 2012 using the Hobo temperature
275 loggers (Sect. 2.2.3). On days during the study period when temperature measurements were
276 available, we applied the average temperature from both measurement locations in the model;
277 when temperature measurements were unavailable, we used Julian Day temperature averages
278 calculated from data from the entire measurement period. We used a Q_{10} value for
279 methanogenesis of 2.4 from Kelly and Chynoweth (1981) to scale the average diffusive flux
280 calculated from both sediment cores from Vault L. on each day of the study period, depending on
281 the sediment temperature in Goldstream L. We assumed that the diffusive flux calculated from
282 measurements was representative of the in-situ diffusive flux at 2 ˚C, the temperature of the
283 cores before analysis. Calculated daily fluxes are shown in Fig. B2. We acknowledge that there
284 is uncertainty in our calculated sediment diffusion rate for the following reasons: (1) In reality, a
285 greater rate of methanogenesis in surface sediments may correspond to a greater proportion of
286 CH_4 escaping via ebullition instead of diffusion; the rate of methanogenesis may scale differently
287 than the rate of diffusion as temperature varies. (2) The diffusive flux of CH_4 is usually very
288 variable across the lake bottom, and our calculations for Goldstream L. are based on the average
289 flux calculated from only two cores from Vault L.

290 **2.3 Modeling**

291 **2.3.1 Overview**

292 Our model simulates the processes that influence CH_4 transport through Goldstream L.
293 during the two-year period in which primary field measurements were collected. Bubbles,
294 released from seeps as observed (Sect. 2.2.6), are either trapped beneath lake ice or released to
295 the atmosphere. Some CH_4 dissolves out of bubbles before they are encapsulated by growing ice.
296 The model water column is resolved into two layers ("upper" and "lower"), divided at 1.25 m
297 below the lake surface, because measured CH_4 concentrations varied independently in these
298 layers during spring ice-melt periods. Changes in the dissolved CH_4 concentration in the lake's
299 water column were driven by dissolution from bubbles trapped beneath ice, aerobic
300 methanotrophy, atmospheric CH_4 emission from freezing water on the ice surface during winter
301 "flooding events" (Sect. 2.3.2), dissolved CH_4 diffusion to the atmosphere in spring and summer,
302 and lake overturn events. CH_4 diffused into the lower layer of the water column from sediments
303 at a constant rate determined from measurements (Sect. 2.2.10).

304 **2.3.2 Ice growth**

305 The rate of black ice growth, which determines how quickly bubbles become
306 encapsulated, is calculated based on a diffusive energy balance model from the steady-state
307 temperature profile through snow and ice on the lake surface. Setting the surface temperature to
308 the observed air temperature and the temperature at the ice-water interface to 0 ˚C yields the
309 following formula for the daily change in black ice thickness:

310 $$\Delta z_b = \alpha^2 \frac{\Delta t}{\rho_i \, \Delta H_{fus}} \times \frac{0\ ^\circ C - T_{air}}{\frac{z_b}{k_i} + \frac{z_w}{k_i} + \frac{z_s}{k_s}} \quad (2)$$

where Δt is 1 d; ρ_i is the ice density (913 kg m^{-3}; Duguay et al., 2003); ΔH_{fus} is the enthalpy of fusion for water (334 J g^{-1}); T_{air} is the mean daily air temperature; z_b, z_w, and z_s are the thicknesses of black ice, white ice, and snow, respectively; k_i and k_s are the thermal conductivities of ice (2.034 W m^{-1} K^{-1}; Duguay et al., 2003) and of snow, respectively. α is a parameter included to account for other processes, such as wind and solar irradiation, following Ashton (1986).

Equation (2) is inaccurate when the snow/ice layer is thin, so Equation (3) was used to calculate z_b when snow and white ice are absent:

$$z_b = \alpha \sqrt{\frac{2\,k_i}{\rho_i\,\Delta H_{fus}} \int (0\ ^\circ C - T_{air})\,dt} \qquad (3)$$

where T_{air} is integrated over time since freeze-up. This formula represents an analytical solution to the differential equation describing black ice growth (of which Eq. (2) is the discretized form) and was applied before the first date of observed snowfall.

The assumptions underlying Eqs. (2) and (3) are invalid for $T_{air} > 0$, which was the case on four consecutive days in October 2010 after freeze-up, but we applied this model as an approximation. Previous studies of melting ice found the formation of channels within lake ice instead of decreasing thickness (e.g. Browman, 1974; Nye, 1989; Jakkila et al., 2009), so we assume zero ice growth around trapped bubbles during this period.

The snow's thermal conductivity was calculated from its density (Sturm et al., 1997), which was estimated from measurements of precipitation and snow depth (Sect. 2.2.8). We assumed that decreases in measured snow depth resulted only from compaction and not sublimation, which resulted in our underestimating the maximum black ice thickness by at most 9 cm (Liston and Sturm, 2002).

333 Occasionally, the weight of snow depresses the ice surface beneath the water level,
334 causing lake water to flood the ice surface and form white ice (i.e., a "flooding" event). The
335 white ice thickness was increased during such events according to the thickness of water required
336 to balance the weight of the snow/ice layer:

337 $$\Delta z_w = \frac{\rho_i}{\rho_w \ \rho_s}(z_s \ \rho_s - z_i \ \rho_i - z_i \ \rho_w) \quad (4)$$

338 where ρ_s and ρ_w are the densities of snow and water, respectively. The volume, V_{flood}, and CH_4
339 concentration of water involved in each flooding event determined the amount of CH_4 released to
340 the atmosphere:

341 $$V_{flood} = \Delta z_w \ A \left(1 - \frac{\rho_s}{\rho_i}\right) \quad (5)$$

342 where A is the lake area (10,030 m^2).

343 The daily change in lake snow depth was calculated as the change in the measured snow
344 depth on land minus Δz_w. An α value of 0.95 yielded the best fit to the measured total ice
345 thickness during the winter of 2011–2012 (Fig. 5d). A second model was constructed for 2010–
346 2011 in which the snow density was set to 450 kg m^{-3} (Bohren and Beschta, 1979; Fancy and
347 White, 1985) on days when the measurement site was visited so that modeled thicknesses could
348 be compared to measured ice thicknesses at the disturbed (artificially compacted) site. An α
349 value of 0.94 yielded the best fit to these data (Fig. 6). Due to the similarity of α values during
350 both winter periods and the greater number of measurements in 2011–2012, an α value of 0.95
351 was used to calculate undisturbed ice thicknesses in the model.

352 **2.3.3 Methane dissolution from bubbles**

353 The model uses Eq. (1) with 60-s time steps to simulate CH_4 diffusion from trapped
354 bubbles into the upper layer of the water column. We calculated that typical ebullition bubbles in

355 Goldstream L. (6.3 ± 0.2 mm bubble diameter measured at the lake surface, mean ± standard
356 deviation, n = 433) lose < 1% of their CH_4 during their ascent through the ≤ 2.9 m water column
357 (Woolf and Thorpe, 1991; Holocher et al., 2003), which is significantly less than the difference
358 in CH_4 contents of fresh and encapsulated bubbles (Sect. 2.2.6). Methane dissolution from rising
359 bubbles was therefore neglected, an approximation similarly employed by Stepanenko et al.
360 (2011).

361 The shapes of trapped bubbles at each seep site determine the area over which CH_4
362 dissolves out. All ebullition bubbles at each site are modeled as a single gas pocket. We tested
363 this approximation by modeling multiple pockets at each site (20 at A-seep sites and 10 at B-seep
364 sites, representative of the number of bubbles found at typical sites in these seep classes), and
365 found that this had a negligible (< 0.5%) effect on the total amount of CH_4 that dissolved into the
366 water column during the ice-cover periods.

367 At each seep site, the model tracks the growth of a cavity within the ice layer, caused by
368 the localized inhibition of ice growth. If the total volume of gas exceeds the cavity's volume, the
369 gas beneath the ice-water interface is modeled as a cylinder. At A, B, and C seep sites, the height
370 of this cylinder is 5.7 mm, as informed by measurements of air bubbles of known volume that we
371 artificially introduced beneath the ice in Goldstream L. The cylinder's radius determines that of
372 the cavity as the ice grows downward. The cylinder's volume and radius decrease as CH_4
373 diffuses out and the ice grows downward, causing cavities to taper at the bottom. At the
374 beginning of each day, a bubble is added to the site, with a CH_4 composition and volume
375 determined from measurements (Sect. 2.2.6). When no gas remains beneath the ice-water
376 interface, the site's bubbles are considered encapsulated. Since the rate of gas diffusion in ice is
377 typically negligible compared to that in water (Hemmingsen, 1958), we assumed that the CH_4

content of bubbles remained constant after encapsulation. Figure 7a summarizes this component of the model.

At Hotspot seep sites, warmer water brought to the surface by frequent ebullition events inhibits ice growth and affects the shapes of cavities. Following Zimov et al. (2001), Hotspot sites were opened to the atmosphere when the daily maximum air temperature exceeded –15 ˚C. The shape of Hotspot cavities was determined by averaging measurements of three cavities in Goldstream L. The bottom radius of the cavity determined the radius of the cylinder beneath the ice-water interface. Bubbles were added to Hotspot seep sites every 8 min, according to our field observations. We found that changing this interval to 1 min and 20 min, both within the range of variability of our observations, affected the total amount of CH_4 that dissolves annually from of hotspot bubbles by no more than 0.05%. Hotspot cavities never closed at the bottom, and when the total volume of gas was less than the cavity volume, the cavity's interior shape determined the area of gas exposed to lake water (Fig. 7b).

2.3.4 Release of ice-trapped bubbles

The "spring ice-melt period" begins on the first day of above-freezing air temperatures and ends on the observed ice-off date. During this period, vertical melt channels spanning the ice layer form between black ice crystals with horizontal c-axes and tend to grow larger as melt progresses, facilitating the transport of water and trapped gas (Browman, 1974). The absorption of solar radiation within the ice layer accelerates this process, particularly after the high-albedo snow cover has melted completely (Williams, 1969; Ashton, 1986; Jakkila et al., 2009), as does the presence of ice-trapped bubbles (our observation when harvesting ice blocks; A. Bondurant pers. comm., 2014). Time-lapse photos indicate significant spatial and temporal variability in the

surface albedo of Goldstream L. during the spring melt period, suggesting that ice permeability was also highly variable.

Ebullition seeps can open prior to ice-off when water pressure breaks ice separating encapsulated bubbles (Zimov et al., 2001). In agreement with the findings of Sasaki et al. (2009), we observed the opening of ebullition seeps throughout the thaw period, indicated by (1) open holes in ice at the locations of former ice-trapped bubbles; (2) rapid, but short-lived (usually < 1 min, but occasionally > 10 min) streams of bubbles escaping from ice through puddles of water on the ice surface; and (3) the lack of gas escape from gas pockets in ice when punctured with an ice spear. We observed that seep sites with higher ebullition flux opened earlier, presumably due to thinner ice between encapsulated bubbles. On each day, the number of open seep sites in each class was increased according to a release rate function informed by these field observations (Fig. B3). Bubble dissolution at closed sites during this period was simulated assuming a zero ice growth rate.

2.3.5 Water column dissolved gases

During the winter ice-cover periods of the model, we assume that dissolved CH_4 is excluded from water as it freezes. This is consistent with observations of CH_4 concentrations in boreal lake ice 10 to 100 times lower than in the underlying water column (Phelps et al., 1998). In some cases, the exclusion of dissolved CH_4 from downward-growing ice leads to the formation of millimeter-scale-diameter tubular bubbles within ice (Adams et al., 2013; Boereboom et al., 2012). Such bubbles were not obvious to us in ice blocks from Goldstream L., so the model did not include this process. We assume no gas exchange between the water column and the atmosphere during the winter ice-cover periods except for the release of dissolved CH_4 from water on the ice surface during flooding events (Sect. 2.3.2).

423 The rate of CH_4 consumption by methanotrophy, r, was calculated according to a double
424 Monod equation (Van Bodegom et al., 2001):

425 $$r = r_{max}\left(\frac{[CH_4]}{K_{S,CH4}+[CH_4]}\right)\left(\frac{[O_2]}{K_{S,O2}+[O_2]}\right) \quad (6)$$

426 where $[CH_4]$ and $[O_2]$ denote the concentrations of dissolved CH_4 and O_2, respectively, r_{max} is the
427 potential maximum methanotrophic rate, and $K_{S,CH4}$ and $K_{S,O2}$ are the affinity constants for CH_4
428 and O_2, respectively. We used a $K_{S,CH4}$ of 0.110 mg L^{-1} (Liikanen et al., 2002; Lofton et al.,
429 2014), a $K_{S,O2}$ of 0.672 mg L^{-1} (Lidstrom and Somers, 1984), and an estimated r_{max} of 0.48 mg
430 L^{-1} d^{-1} based on measurements in Goldstream L. by Martinez-Cruz et al. (2014). In both years of
431 the model, dissolved O_2 was depleted within 60 days of freeze-up, after which the
432 methanotrophic rate was essentially zero until the spring ice-melt period (Fig. 8b). Measured O_2
433 concentrations followed a similar trend as modeled O_2 concentrations during the ice-cover
434 periods. We assumed uniform water column CH_4 and O_2 concentrations in the winter before the
435 spring ice-melt periods, as we found that imposing the vertical gradients observed in our field
436 measurements would have minor effects on the magnitude of CH_4 dissolution from bubbles and
437 the magnitude of CH_4 emissions from flooding events. Our field measurements suggest that
438 assuming uniform concentrations resulted in our underestimating the magnitude of CH_4
439 emissions from flooding events during the study period by approx. 5%.
440 The rate of water-atmosphere gas exchange during ice-melt depends on the extent of ice
441 permeability and the advection of water through ice, both of which are poorly constrained. The
442 methanotrophic rate depends on the availability of dissolved O_2, which is spatially irregular.
443 Furthermore, methanotrophy sometimes does not resume until after an “induction period”
444 following the reintroduction of O_2. Induction periods of 0 to 20 d have been observed in soils and
445 in Arctic lakes (Bender and Conrad, 1995; Dunfield et al., 1999; Martinez-Cruz et al., 2014).

446 To account for these uncertainties, the model includes two parameters adjusted to fit
447 modeled amounts of dissolved CH_4 and O_2 during the spring ice-melt periods to measurements
448 (Fig. 8). The amount in moles of CH_4, R, released to the atmosphere on each day by diffusion
449 from the upper 1.25 m of the water column was calculated as follows:

450 $$R = s\, p_1\, D_{CH4}\, ([CH_4] - [CH_4]_{eq}) \quad (7)$$

451 where s is the total number of seep sites open to the atmosphere, p_1 is an adjustable parameter
452 (with units m s site^{-1}), and $[CH_4]$ represents the average modeled CH_4 concentration in the upper
453 layer. The amount of O_2 diffusing into the upper layer from the atmosphere was calculated with
454 the same p_1 and s parameters. As suggested by field measurements, O_2 did not diffuse into the
455 lower layer (deeper than 1.25 m). The rate of CH_4 consumption was calculated according to Eq.
456 (6) and scaled by the second adjustable parameter.

457 We did not observe a decrease in dissolved CH_4 or an increase in O_2 in the hypolimnion
458 of Goldstream L. immediately following ice-off, suggesting that the water column remained
459 stratified as surface temperatures increased. Others have similarly observed water column
460 stability in Arctic lakes during and after spring melt, which they attributed to intense solar
461 radiation and the inflow of meltwater from surrounding areas (Bergmann and Welch, 1985;
462 Burn, 2002; Bastviken et al., 2004). Measured CH_4 concentrations in the upper 1 m of the water
463 column increased significantly during a period of approx. 12 days in early May 2012 spanning
464 the date of observed ice-off, suggesting significant upper-layer mixing during that time.
465 Measured temperature profiles indicate a similar phenomenon in May 2011. As an
466 approximation, all CH_4 in the upper layer of the water column was released to the atmosphere
467 over a period of five days following ice-off.

468 The rate of dissolved CH_4 diffusion to the atmosphere during the ice-free period was
469 calculated by multiplying the difference between the measured surface CH_4 concentration and
470 the equilibrium CH_4 concentration on each day by a "gas-transfer coefficient," k. We used a k
471 determined empirically by Cole and Caraco (1998), representing an average k for the open-water
472 period at Mirror Lake, a low-wind temperate lake. We converted it appropriately using a Schmidt
473 number for CH_4 at 10 ˚C of 1052 (Wania et al., 2010), which gave a k for CH_4 of 1.82 cm h^{-1}. As
474 we did not measure wind velocities at Goldstream L. during the study period, we were unable to
475 apply the wind-dependent parameterization of k presented by Cole and Caraco (1998). However,
476 we believe this did not significantly affect our results for two reasons: (1) Goldstream L. is
477 surrounded by trees, suggesting that wind speeds there are similar to those at the low-wind lake
478 measured by Cole and Caraco, and (2) Cole and Caraco noted that k is relatively independent of
479 wind speed at low wind speeds, suggesting that any difference in average wind speed between
480 Mirror L. and Goldstream L. would not have appreciably affected the value of k. The value of k
481 we used differed by 2% from that applied by Kling et al. (1992) to lakes on the northern coastal
482 plain of Alaska, which are presumably windier than Goldstream L. Kling et al. noted that they
483 likely underestimated the rate of gas diffusion from these lakes, suggesting that applying this
484 value of k for Goldstream L. is justified.

485 Measured concentrations from 2012 were used during the summer of 2011 because
486 surface CH_4 concentrations were not measured in 2011. The similarities between CH_4
487 concentration-depth profiles obtained during both open-water periods (Fig. 9) suggest that
488 surface CH_4 concentrations were also similar. The mean daily rate of CH_4 diffusion to the
489 atmosphere during both open-water periods (1.2 mmol m^{-2} d^{-1}) was within the range of
490 observations for other boreal lakes (Phelps et al., 1998; Huttunen et al., 2003; Walter et al.,

491 2006). We assumed that CH_4 not emitted to the atmosphere during this period was consumed by
492 methanotrophy.

493 During the summer of 2011, our measurements of water temperature, dissolved CH_4, and
494 dissolved O_2 indicated a gradual deepening of the epilimnion in Goldstream L. (Fig. 9). On 6
495 October 2011, we observed uniform depth profiles for all of these variables, low (< 3 μM)
496 dissolved CH_4 concentrations, and high (156 mM) O_2 concentrations, suggesting that fall
497 overturn had occurred by then. Similar trends in temperature and dissolved O_2 concentrations
498 were observed during the open-water period in 2012. Surface O_2 concentrations remained high
499 throughout this period in 2011 while surface CH_4 concentrations remained low, suggesting that
500 methanotrophy in the upper layer of the water column prevented the significant release of CH_4
501 dissolved in the hypolimnion to the atmosphere before and during overturn. Kankaala et al.
502 (2007) similarly estimated that the majority (83–88%) of dissolved CH_4 in the hypolimnion of a
503 lake in Finland was consumed by methanotrophy during fall overturn. The amount of dissolved
504 CH_4 before freeze-up was set to 0, as suggested by our measurements, and the amount of
505 dissolved O_2 was determined from measurements.

506 **2.4 Statistical analysis**

507 Heteroscedastic t-tests were performed using Excel (Microsoft, Redmond, Washington,
508 USA).

509

510 **3 Results and discussion**

511 **3.1 Evidence of bubble dissolution**

512 Our model of CH_4 dissolution from submerged, gas-filled mesocosm chambers (Sect.
513 2.2.7) suggests that a significant amount of CH_4 dissolves out of bubbles on the timescale of

514 bubble encapsulation (days to months). This model agrees with measured volumes and CH_4
515 compositions of gas in chambers, except at 145 and 165 hours in the fall trial (Fig. 4). We
516 observed defects in the ebullition deflectors on those chambers, and our weather observations
517 indicate a decrease in barometric pressure prior to 145 hours, which is known to induce
518 ebullition events (Mattson and Likens, 1990). We therefore attribute these discrepancies to the
519 addition of natural ebullition bubbles.

520 Measurements of CH_4 concentrations in bubbles trapped within the ice layer also indicate
521 significant dissolution. At C seep sites, "fresh" bubbles collected immediately after their ascent
522 through the water column (Sect. 2.2.6) had significantly greater CH_4 concentrations than
523 encapsulated bubbles (85% vs. 72%, t-test, $p < 0.05$). However, we did not find significant
524 differences between the concentrations of encapsulated vs. "fresh" A- and B-type bubbles due to
525 a paucity of field measurements (zero and two encapsulated A- and B-type bubbles were
526 sampled, respectively).

527 **3.2 Baseline results**

528 Both the model as described in Sect. 2.3 (the "Baseline" version) and our measurements
529 indicate that dissolved CH_4 accumulates in Goldstream L. throughout the ice-cover periods,
530 reaching maxima approximately one month prior to ice-off (Fig. 8a). The measured maximum
531 concentrations (400 μM and 337 μM in 2011 and 2012, respectively) are within the range of
532 measurements for other lakes in Alaska (Phelps et al., 1998). Figure 10 shows the relative
533 contributions of all sources of dissolved CH_4 in the model.

534 We calculated annual atmospheric CH_4 emissions by five distinct mechanisms: (1) The
535 direct release of bubbles from open ebullition seep sites ("Direct Ebullition"), (2) the release of
536 free-phase gas trapped by the ice layer ("IBS"), (3) emission during winter "Flooding" events

537 (Sect. 2.3.2), (4) "Diffusion" of dissolved CH_4 from the water column, and (5) emission during
538 partial lake overturn events ("Overturn"). Bastviken et al. (2004) referred to the fifth mechanism
539 as "storage flux," but we termed it "Overturn" to distinguish it from the release of "stored" CH_4
540 by diffusion through open ebullition seep sites during the spring melt period prior to lake
541 overturn. Figure 11 shows emissions from the entire surface of Goldstream L. by each of these
542 modes.

543 Periods of zero emissions correspond to periods of atmospheric temperatures below –15
544 ˚C, when Hotspot seeps in the model were closed. When Hotspot seeps reopened, IBS emissions
545 peaked due to the sudden release of gas within cavities. In reality, other factors, including
546 ebullition rates and ice morphology, govern the opening and closing of Hotspot seep sites, so
547 Hotspot IBS emissions may actually be distributed more evenly throughout the ice cover period.
548 This is a potential reason for why peaks in the measured atmospheric CH_4 concentration
549 occurred more frequently than peaks in Hotspot IBS emissions during the winter of 2010–2011
550 (Fig. 11b). For this reason, and because there are no field observations to validate our
551 representation of the geometry of gas beneath the ice-water interface at Hotspot seep sites, our
552 estimates of the magnitude and timing of Hotspot IBS emissions are likely uncertain. The
553 average daily rate of atmospheric CH_4 emissions was highest during the spring ice-melt periods
554 (70 mol CH_4 d^{-1}) due to emission of dissolved and trapped free-phase CH_4, and lowest during the
555 winter ice-cover periods (24 mol CH_4 d^{-1}) due to the impediment of ebullition bubbles by lake
556 ice. The atmospheric CH_4 concentration measured above Goldstream L. peaked significantly in
557 early April 2011, when modeled IBS emissions also peaked (Fig. 11b). This supports our
558 representation of bubble release prior to ice-off in the model (Sect. 2.3.4). A period of elevated
559 atmospheric concentrations prior to ice-off was also observed in 2010. On average, 75% and 8%

560 of annual atmospheric CH_4 emissions occurred via Direct Ebullition and IBS, respectively,
561 during the two-year study period (Fig. 11). IBS emissions constituted 6% and 9% of annual
562 emissions from Goldstream L. in each year (2010–2011 and 2011–2012, respectively).
563 The majority (67%) of CH_4 released annually from the bottom sediments of Goldstream
564 L. by ebullition seeps in the model was emitted directly to the atmosphere, unimpeded by lake
565 ice (Fig. 12a). This proportion is determined primarily by the ebullition flux from Hotspot seeps,
566 which remain open to the atmosphere throughout much of the ice cover period. Ebullition from
567 Hotspot seeps constitutes 48% of the total annual seep ebullition flux from sediments in
568 Goldstream L. Efforts to improve estimates of CH_4 emissions from Goldstream L. should
569 therefore focus first on Direct Ebullition emissions, particularly those from Hotspots. Our
570 estimate of Direct Ebullition is conservative because it does not include ebullition from non-seep
571 "background" locations. Walter et al. (2006) found that "background" ebullition comprises 25%
572 of total annual CH_4 emissions from two Siberian thermokarst lakes and was highest in the
573 summer, when microbes in warm surface sediments produce CH_4 that is released from non-seep
574 locations. Our preliminary data from bubble traps over non-seep locations, as identified by
575 bubble-free ice in the early winter, suggest that background ebullition also occurs in Goldstream
576 L.
577 The model indicates that seasonal ice cover effectively impedes the release of ebullition
578 CH_4 to the atmosphere. During the ice-cover period, 44% of CH_4 bubbling from sediments
579 dissolved into the water column when bubbles were trapped by ice. Conversely, 45% was
580 released by Direct Ebullition from Hotspots and A, B, and C seep sites open during spring melt,
581 and 11% was trapped as free-phase gas by ice. On an annual basis, 7% percent of the total seep

582 ebullition flux was trapped as IBS and later released to the atmosphere when ice melted. The
583 majority of IBS emissions was associated with Hotspots reopening in the winter (Fig. 12a).
584 Of the CH_4 in seep ebullition bubbles impeded by lake ice, 80% ultimately dissolved into
585 the water column, and 56% of this dissolved CH_4 was consumed by methanotrophy (Fig. 12b). In
586 the model, the extent of winter methanotrophy is determined entirely by the amount of O_2
587 dissolved in the water column at the time of freeze-up. Eighty-two percent of the total amount of
588 CH_4 emitted annually from the sediments of Goldstream L. by seep ebullition and diffusion
589 reached the atmosphere without being oxidized (Table 1). Because the amount of CH_4 that
590 dissolves out of bubbles during the ice cover period is much greater than the amount that diffuses
591 out of sediments (Fig. 10), ice cover facilitates substantially greater CH_4 dissolution into the
592 water column and therefore increased methanotrophy.
593 The shapes of ebullition bubbles in harvested ice blocks (Sect. 2.2.6) varied greatly,
594 depending on the seep type, ice growth rates, and the degree of bubble coalescence. Individual
595 bubbles often tapered at the bottom, but vertically joined bubbles sometimes had tapering tops
596 (Fig. 12c). For comparison with observations, the bubble dissolution component of the model
597 was executed in isolation to simulate CH_4 dissolution from a single trapped bubble, assuming a
598 constant ice growth rate and zero dissolved CH_4 concentration. We fit the shapes of modeled
599 bubbles to measurements by adjusting the ice growth rate and initial volume. Results agreed
600 reasonably with measurements of bubbles that tapered at the bottom, and fits were better for
601 bubbles with more concave sides (Fig. 12a). Bubble radii calculated assuming a constant
602 dissolved CH_4 concentration of 387 μM, the maximum concentration observed during the study
603 period, differed from those in our original results by no more than 1 mm, suggesting that bubble
604 shapes are more strongly influenced by the ice growth rate than the rate of CH_4 dissolution.

605 Discrepancies between calculated and measured shapes likely arose from fluctuations in the ice
606 growth rate and the error associated with modeling gas beneath the ice-water interface as a
607 cylinder with constant height.

608 In the model, the decrease in bubble volume due to CH_4 dissolution gives rise to the
609 shape of bubbles that taper at the bottom, so no bubbles had flat bottoms or tapering tops. We
610 attribute observations in lake ice blocks of the occasional formation of bubbles with this opposite
611 orientation to the insulating effect of gas frozen within the ice layer (Engram et al., 2013), which
612 causes ice around trapped bubbles to grow faster than ice directly beneath, giving rise to dome-
613 shaped or conical cavities at ebullition seep sites. This effect may compete with the effect of
614 volume loss to determine bubble shapes, therefore causing a distribution of both orientations.
615 Further investigation is needed to determine the effect of localized ice growth inhibition on
616 bubble shapes and CH_4 dissolution.

617 Modeled CH_4 concentrations of encapsulated bubbles did not differ significantly from
618 measurements for bubbles at B and C seep sites (t-tests, $p > 0.05$); however, only two
619 encapsulated B-type bubbles and four C-type bubbles were sampled from Goldstream L. To
620 increase the sample size, we also compared modeled concentrations to measurements of 30
621 encapsulated bubbles from four other thermokarst lakes in interior Alaska, the northern Seward
622 Peninsula in Alaska, and northern Siberia (Walter et al., 2008; Sepulveda-Jauregui et al., 2014b).
623 It was often impossible to classify ebullition sites beneath white ice during the spring ice-melt
624 period as A, B, or C, so measurements from all ebullition classes were pooled and adjusted to
625 account for observed differences in "fresh" bubble CH_4 concentrations among lakes (Sepulveda-
626 Jauregui et al., 2014b). The mean adjusted concentration in encapsulated bubbles from other
627 lakes (58%) did not differ significantly from those measured in Goldstream L. (68%; t-test, p >

628 0.05), but the mean adjusted concentration for all five lakes, (60%) was significantly lower than
629 modeled concentrations (69%; t-test, $p < 0.05$).

630 As a sensitivity analysis, we also constructed a version of the model, "Episodic
631 Ebullition," in which individual seep fluxes, rather than smoothed fluxes, were applied during
632 the ice-cover periods in the model. We found that encapsulated bubbles in the "Episodic
633 Ebullition" version had a mean CH_4 concentration (32%) significantly less than both the mean
634 measured concentration for all five lakes and the mean modeled concentration when smoothed
635 fluxes were applied (t-tests, $p < 0.001$). The larger surface area, on average, of trapped gas
636 pockets at non-Hotspot seep sites in the "Episodic Ebullition" version allowed more CH_4 to
637 dissolve out after individual ebullition events, despite the fact that gas pockets were encapsulated
638 faster by ice (due to extended periods of no ebullition). Consequently, IBS emission from A, B,
639 and C seep sites was 28% less than in the "Baseline" version. The "Episodic Ebullition" version
640 appeared to underestimate encapsulated bubble CH_4 concentrations in comparison to
641 observations from the five thermokarst lakes. Likely reasons for this are that we assume the 5.7
642 mm bubble height measured on 20–40 mL gas pockets applies to all bubbles, but a 5,000 mL
643 ebullition event, which can occur in the "Episodic Ebullition" version, produces larger gas
644 pockets with possibly different bubble heights. Secondly, we did not account for lateral
645 migration of bubbles beneath ice in the model.

646 Results suggest that our slight overestimation of encapsulated bubble CH_4 concentrations
647 in the "Baseline" version of the model arises from our applying smoothed ebullition fluxes.
648 However, applying smoothed ebullition fluxes is justified for three reasons: (1) The magnitude of
649 CH_4 dissolution into the water column in the model was more sensitive to the magnitude of the
650 CH_4 ebullition flux during the ice-cover period than the timing of this release. This magnitude is

651 more accurately represented by the larger sample size of measured seep fluxes that informed our
652 calculation of smoothed fluxes. (2) The majority of CH_4 in bubbles impeded by lake ice
653 dissolves into the water column (Fig. 12), so major discrepancies in the mean CH_4 concentration
654 of encapsulated bubbles (69% "Baseline" vs. 32% "Episodic Ebullition") result in only minor
655 discrepancies in the magnitude of CH_4 dissolution into the water column and therefore in the
656 magnitude of annual CH_4 emissions. In the "Episodic Ebullition" version, the total magnitude of
657 CH_4 dissolution from bubbles trapped at A, B, and C seep sites and the total annual CH_4
658 emissions from Goldstream L. were, respectively, 2.5% and 5.3% greater than those in the
659 "Baseline" version (Fig. A1). (3) It is more computationally efficient to execute the model using
660 smoothed fluxes than with a large number of individual seeps.

661 **3.3 Additional "Tinies" ebullition seeps**

662 Our field observations indicate a previously undefined class of ebullition seeps, "Tinies,"
663 in Goldstream L. Bubbles released from Tinies seeps are trapped beneath lake ice typically
664 without lateral merging (similar to A-type bubbles). However, unlike individual A, B, C, and
665 Hotspot seeps, which have a more focused point of release and sites with tightly clustered and/or
666 coalesced ice-bubbles (usually less than 0.8 m^2 in area), Tinies bubbles are typically found in
667 patches that span several square meters. Most Tinies seeps release bubbles throughout the winter
668 (K. M. W. A., unpublished data). Preliminary measurements indicate that Tinies seeps occupy
669 approximately 1.4% of the area of Goldstream L. and that including ebullition from Tinies seeps
670 would increase our estimate of total seep ebullition in Goldstream L. by 2 to 9%. We estimate
671 that including these seeps in the model would result in a 2% increase in the amount of dissolved
672 CH_4 in Goldstream L. during the ice cover periods, although this estimate is uncertain due to a

673 lack of constraints on our representation of Tinies in the model. These results warrant further
674 investigation and characterization of Tinies seeps.

675 **3.4 Sensitivity analysis**

676 Because of the many approximations in the formulation of the model, its output often
677 differed from measurements. These discrepancies informed the construction of additional
678 modified versions of the model used to estimate uncertainties in our results arising from these
679 approximations. The modifications in these versions are summarized in Table 1, and their results
680 are discussed in detail in Appendix A. Our findings imply two key conclusions. (1) Secondary
681 processes that influence the dissolved CH_4 concentration in Goldstream L. during the ice-cover
682 periods, such as CH_4 diffusion from bottom sediments and methanotrophy, do not appreciably
683 affect the magnitudes of IBS emissions. (2) The magnitudes of CH_4 emission and oxidation
684 during spring ice-melt and summer open-water periods are not well constrained in the model,
685 and further investigation of these processes is therefore necessary.

686 **3.5 Future climate change**

687 We constructed a "Warmer Climate" version of the model, in which air temperatures
688 were increased uniformly by 5 ˚C, to simulate future climate change. The only processes in the
689 model affected were ice growth and the closing of Hotspot seep sites to the atmosphere. In this
690 version, freeze-up was delayed by 15 and eight days in 2010 and 2011, respectively, and the
691 average yearly maximum ice thickness was 12% less than in the Baseline version. The resulting
692 increase in total atmospheric emissions was driven primarily by a 7% increase in Direct
693 Ebullition emissions arising from shorter ice-cover periods and fewer days on which Hotspots
694 were closed (Fig. A1c). Less CH_4 dissolved into the water column from ebullition seep sites
695 despite slower ice growth, resulting in decreased Diffusion and IBS emissions during the spring

ice-melt periods (Fig. A1b). A greater proportion (85% vs. 82%) of CH_4 released annually from sediments reached the atmosphere than in the "Baseline" version (Table 1). As we did not account for the temperature dependence of methanogenesis, our estimates of the increase in CH_4 emissions due to warming are likely conservative.

4 Conclusions

We present a model of CH_4 transport and emission processes in seasonally ice-covered lakes, focusing primarily on CH_4 dissolution from bubbles trapped beneath lake ice and "ice-bubble storage" (IBS) emissions. Close agreement between the model's output and our field measurements suggests that our model accurately represents many of these processes in Goldstream L. and other thermokarst lakes.

IBS emissions constituted 8% of total annual emissions from Goldstream Lake during the two-year study period. This quantity is primarily determined by ebullition and lake ice growth; it is insensitive to the amount of dissolved CH_4 because the water column CH_4 concentration is typically undersaturated relative to concentrations in bubbles. On an annual basis, a majority of CH_4 in ebullition bubbles in the model is released directly to the atmosphere, unimpeded by lake ice. Methanotrophy determines the extent to which lake ice reduces net atmospheric CH_4 emissions. In the model, the magnitudes of methanotrophy during the winter and summer periods are constrained by measurements of dissolved gases. The magnitude of spring methanotrophy was not well constrained due to uncertainties in the timing of CH_4 release from trapped ebullition seep sites, the rate of water-atmosphere gas exchange, and the possible "induction period" of methanotrophy. The amount of dissolved CH_4 subject to methanotrophy during spring ice-melt is significant (21% of CH_4 released annually by diffusion and ebullition from the sediments of

719 Goldstream L.), so further investigation is needed to reduce this source of uncertainty in
720 calculated CH_4 emissions. Our model indicates that seasonal lake ice increases the amount of
721 CH_4 consumed by methanotrophs by facilitating CH_4 dissolution from ice-trapped bubbles prior
722 to encapsulation. Therefore, shorter ice-cover seasons and less black ice growth simulated in a
723 warmer climate will likely increase CH_4 emissions from northern lakes. The model could be
724 further refined by including the temperature dependence of methanogenesis and the response of
725 lake ice to projected changes in precipitation.
726
727 **Appendix A: Sensitivity analyses**
728 **A1 CH_4 diffusion from sediments**
729 The rate of CH_4 diffusion from sediments in the model is uncertain because it was
730 calculated from measurements in Vault Lake (Sect. 2.2.10), which exhibits greater seep
731 ebullition activity than Goldstream Lake (Sepulveda-Jauregui et al., 2014b), likely because it is a
732 younger thermokarst lake. This suggests the greater availability of substrate for methanogenesis
733 (Kessler et al., 2012) in Vault L. and therefore greater sediment diffusion rates. Furthermore, the
734 diffusion rate in Goldstream L. likely exhibits significant spatial variability, due to differences in
735 substrate availability between its thermokarst and non-thermokarst zones, and temporal
736 variability, due to seasonal variation in sediment temperature, which also influences
737 methanogenesis rates (Whalen, 2005).
738 We constructed a "Less Diffusion" version of the model, in which the diffusion rate from
739 sediments was five times less than in the "Baseline" version, which resulted in a marginal
740 decrease in the modeled amount of dissolved CH_4 in the water column throughout the study
741 period (Fig. 8a). This difference was not substantial because dissolution from trapped bubbles

742 comprised 87% of the dissolved CH_4 sources during the ice-cover periods in the "Baseline"
743 version (Fig. 12). Methanotrophy during the summer periods was considerably reduced (Fig.
744 A1b), and a greater proportion (86% vs. 82% in the "Baseline" version) of CH_4 released from
745 bottom sediments reached the atmosphere (Table 1).

746 Due to lower dissolved CH_4 concentrations throughout the winter and spring in the "Less
747 Diffusion" version, 0.4% more CH_4 diffused into the water column from trapped bubbles.
748 Because the maximum CH_4 concentration in Goldstream L. is generally significantly less than
749 the saturation concentration calculated from the CH_4 concentration within trapped bubbles, the
750 magnitudes of bubble dissolution and IBS emissions are insensitive to the diffusion rate from
751 sediments and other processes that affect the dissolved CH_4 concentration. It may be possible to
752 estimate Ebullition and IBS emissions for lakes similarly undersaturated in dissolved CH_4 using
753 only information about lake ice and ebullition dynamics.

754 **A2 Lake ice thickness**

755 Although the model exhibits good agreement with measured total ice thicknesses, it does
756 not agree as closely with measured white and black ice thicknesses during the ice-cover period
757 (Fig. 5). These measurements are more uncertain than those of total ice thickness due to error
758 associated with observers looking through narrow auger holes in winter for differences in ice
759 color. We constructed two additional versions of the model in which calculated black ice
760 thickness matched the upper and lower extremes of the range of our measurements and the total
761 ice thickness matched measurements (Fig. A2). The snow density was fixed at either 300 or 100
762 kg m^{-3}, resulting in "More Black Ice" or "Less Black Ice," respectively, due to the associated
763 changes in snow conductivity and snow depth. In the "Baseline" version, the average snow
764 density was 180 kg m^{-3}.

765 In the "More Black Ice" version, flooding events (Sect. 2.3.2) were less frequent,
766 resulting in less white ice growth and a 97% reduction in Flooding emissions. At A, B, and C
767 ebullition seep sites, more CH_4 was encapsulated by ice, and 14% less CH_4 dissolved out of
768 trapped bubbles (Fig. A1a). The magnitude of IBS emissions from A, B, and C seep sites was 2.5
769 times greater than in the "Baseline" version. The opposite was true of results from the "Less
770 Black Ice" version.

771 **A3 Diffusively controlled layer thickness**

772 Setting the effective thickness of the diffusively controlled layer, δ_{eff}, to 0.15 mm and
773 0.35 mm in the model of CH_4 dissolution from submerged chambers (Sect. 2.2.7) yielded
774 reasonable fits to measured volumes and CH_4 concentrations for both trials (Fig. 4), so these
775 values were used in two additional versions of the model. At δ_{eff} = 0.35 mm ("Greater δ_{eff}"), 5%
776 less CH_4 dissolved into the water column from bubbles, which resulted in greater IBS emissions
777 and less emission of dissolved CH_4 during the spring ice-melt period (Fig. A1). The opposite was
778 true for results from the "Lesser δ_{eff}" version (δ_{eff} = 0.15 mm). 83% and 81% of CH_4 reached the
779 atmosphere in the "Greater" and "Lesser δ_{eff}" versions, respectively (Table 1).

780 **A4 Methane emissions during spring melt**

781 The model does not include biological processes that consume or produce O_2 during the
782 spring ice-melt period, which could significantly impact the magnitude of CH_4 oxidation during
783 this period. Furthermore, the timing of the release of trapped gas represented in the model may
784 differ from reality due to the paucity of field observations of this timing. Consequently, the
785 magnitudes of CH_4 diffusion to the atmosphere and methanotrophy during the spring ice-melt
786 periods in the model are uncertain. In the "Baseline" version of the model, the amount of CH_4
787 that dissolves into the water column from ebullition seep sites and sediments during the winter

788 and spring periods, minus the amount oxidized during the winter periods, represents 21% of the
789 total CH_4 budget for Goldstream L. Methanotrophs consume 17% of this dissolved CH_4 during
790 the spring and summer periods. Michmerhuizen et al. (1996) found that an insignificant portion
791 of CH_4 dissolved in Minnesota and Wisconsin lakes is oxidized during spring ice-melt. If we
792 similarly assumed no methanotrophy during the spring ice-melt periods in the model, Spring
793 Diffusion emissions would increase by a factor of 2.8, and total atmospheric emissions during
794 the study period would increase by 4.3%.

795 We constructed two versions of the model ("Early" and "Late Release"), in which gas
796 trapped at A, B, and C seep sites was released to the atmosphere on the first or last day of the
797 ice-melt periods, respectively, to evaluate the impact of uncertainties in our release rate functions
798 (Sect. 2.3.4). In the "Late Release" version, 4.4 times more CH_4 dissolved from trapped bubbles
799 during the spring ice-melt periods than in the "Baseline" version, resulting in decreased IBS
800 emissions from non-Hotspot seep sites and increased Overturn emissions (Fig. A1). Total
801 emissions during the spring ice-melt periods were 26% greater than in the "Baseline" version,
802 and 85% of CH_4 released from bottom sediments throughout the study period reached the
803 atmosphere (Table 1). Results from the "Early Release" version did not differ as much from the
804 "Baseline" version (Fig. A1) because the maxima of our release rate functions occurred close to
805 the beginning of the spring ice-melt period. These findings suggest that the timing of bubble
806 release during the spring-ice melt period can significantly impact spring CH_4 emissions and that
807 further investigation is needed to reduce this source of uncertainty in our results.

808 **A5 Summer CH_4 Diffusion Emissions**

809 There is a significant degree of uncertainty associated with our estimate of the magnitude
810 of Diffusion emissions during the open-water periods in the model, as we did not include the

effect of wind speed on the rate of CH_4 diffusion to the atmosphere, and we used measurements of the surface CH_4 concentration in 2012 to calculate the diffusion rate in 2011 (Sect. 2.3.5). Diffusion emissions during the summer open-water period constitute a relatively small proportion (9%) of total calculated CH_4 emissions from Goldstream L. during the study period. At most, summer Diffusion emissions could increase by a factor of two (in which case no CH_4 is consumed by methanotrophy during the open-water periods). In this case, summer Diffusion emissions would constitute 16% of total emissions, but the magnitudes of IBS and Direct Ebullition emissions would remain unchanged.

Appendix B: Supplementary figures

Author contributions

K. M. Walter Anthony conceived this study. S. Greene designed the model, developed the model code and performed the simulations and data analysis with significant input from all co-authors. S. Greene and K. M. Walter Anthony wrote the manuscript. K. M. Walter Anthony, A. Sepulveda-Jauregui, and K. Martinez-Cruz were responsible for the field and lab experiments. All authors commented on the composition of the manuscript.

Acknowledgements

We thank Amy Strohm for measurements of snow and ice thickness, dissolved gas, temperature, ice-bubble mesocosms and late-winter bathymetry. Dragos Vas, Laura Brosius, Laurel McFadden, Casey Pape, Odin Miller, Prajna Regmi, Allen Bondurant, Joanne Heslop, Melanie Engram, and Peter Anthony also assisted with field and lab work. Christopher Swingley

834 provided climate data from the NWS Co-Op site in Goldstream Valley. Peter Anthony conducted
835 GIS analysis. Martin Jeffries and Frederic Thalasso provided input on the model's design.
836 Melanie Engram and Martin Jeffries provided useful comments on the manuscript. This work
837 was supported by the DOE #DE-NT0005665, NASA Carbon Cycle Sciences #NNX11AH20G,
838 the NASA Astrobiology Institute's Icy Worlds node, and NSF #0732735 and #1107892.
839

840 **References**

841 Adams, E. E., Priscu, J. C., Fritsen, C. H., Smith, S. R., and Brackman, S. L.: Permanent ice
842 covers of the McMurdo Dry Valley Lakes, Antarctica: Bubble formation and metamorphism, in:
843 Ecosystem Dynamics in a Polar Desert: The McMurdo Dry Valleys, Antarctica, Priscu, J. C.
844 (Ed.), American Geophysical Union, Washington, D. C., USA, 281–295,
845 doi:10.1029/AR072p0281, 2013.
846 Ashton, G. D. (Ed.): River and Lake Ice Engineering, Water Resources Publications, Highlands
847 Ranch, Colorado, USA, 1986.
848 Bastviken, D., Cole, J. J., Pace, M. L., Van de Bogert, M. C.: Fates of methane from different
849 lake habitats: Connecting whole-lake budgets and CH_4 emissions, J. Geophys. Res., 113,
850 G02024, doi:10.1029/2007JG000608, 2008.
851 Bastviken, D., Cole, J., Pace, M., and Tranvik, L.: Methane emissions from lakes: Dependence
852 of lake characteristics, two regional assessments, and a global estimate, Global Biogeochem. Cy.,
853 18, GB4009, doi:10.1029/2004GB002238, 2004.
854 Bastviken, D., Tranvik, L. J., Downing, J. A., Crill, P. M., and Enrich-Prast, A.: Freshwater
855 methane emissions offset the continental carbon sink, Science, 331, 50,
856 doi:10.1126/science.1196808, 2011.

857 Bender, M. and Conrad, R: Effect of CH_4 concentrations and soil conditions on the induction of
858 CH_4 oxidation activity, Soil Biol. Biochem., 27, 1517–1527, doi:10.1016/0038-0717(95)00104-
859 M, 1995.
860 Bergmann, M. A. and Welch, H. E.: Spring meltwater mixing in small arctic lakes, Can. J. Fish.
861 Aquat. Sci., 42, 1789–1798, doi:10.1139/f85-224, 1985.
862 Boereboom, T., Depoorter, M., Coppens, S., and Tison, J.-L.: Gas properties of winter lake ice in
863 Northern Sweden: implication for carbon gas release, Biogeosciences, 9, 827–838,
864 doi:10.5194/bg-9-827-2012, 2012.
865 Bohren, C. F. and Beschta, R. L.: Snowpack albedo and snow density, Cold Reg. Sci. Technol.,
866 1, 47–50, doi:10.1016/0165-232X(79)90018-1, 1979.
867 Broecker, W. S. and Peng, T. H.: Gas exchange rates between air and sea, Tellus, 26, 21–35,
868 doi:10.1111/j.2153-3490.1974.tb01948.x, 1974.
869 Browman, L. G.: Channels in ice, in: Advanced concepts and techniques in the study of snow
870 and ice resources, Santeford, H. S. and Smith, J. L. (Comp.), Monterey, California, USA, 2–6
871 December 1973, 224–234, 1974.
872 Burn, C. R.: Tundra lakes and permafrost, Richards Island, western Arctic coast, Canada, Can. J.
873 Earth Sci., 39, 1281–1298, doi:10.1139/e02-035, 2002.
874 Casper, P., Maberly, S. C., Hall, G. H., and Finlay. B. J.: Fluxes of methane and carbon dioxide
875 from a small productive lake to the atmosphere, Biogeochemistry, 49, 1–19,
876 doi:10.1023/A:1006269900174, 2000.
877 Cole, J. J. and Caraco, N. F.: Atmospheric exchange of carbon dioxide in a low-wind
878 oligotrophic lake measured by the addition of SF_6, Limnol. Oceanogr., 43, 647–656, 1998.

879 Duguay, C. R., Flato, G. M., Jeffries, M. O., Ménard, P., Morris, K., and Rouse, W. R.: Ice-cover
880 variability on shallow lakes at high latitudes: model simulations and observations, Hydrol.
881 Process., 17, 3465–3483, doi:10.1002/hyp.1394, 2003.
882 Dunfield, P. F., Liesack, W., Henckel, T., Knowles, R., and Conrad, R.: High-affinity methane
883 oxidation by a soil enrichment culture containing a type II methanotroph, Appl. Environ.
884 Microb., 65, 1009–1014, 1999.
885 Engram, M., Walter Anthony, K., Meyer, F. J., and Grosse, G.: Characterization of L-band
886 synthetic aperture radar (SAR) backscatter from floating and grounded thermokarst lake ice in
887 Arctic Alaska, The Cryosphere, 7, 1741–1752, doi:10.5194/tc-7-1741-2013, 2013.
888 Fancy, S. G. and White, R. G.: Energy expenditures by caribou while cratering in snow, J.
889 Wildlife Manage., 49, 987–993, doi:10.2307/3801384, 1985.
890 Gash, J. H. C.: A note on estimating the effect of a limited fetch on micrometeorological
891 evaporation measurements, Bound.-Lay. Meteorol., 35, 409–413, doi:10.1007/BF00118567,
892 1986.
893 Hamilton, T. D., Craig, J. L., and Sellmann, P. V.: The Fox permafrost tunnel: a late Quaternary
894 geologic record in central Alaska, Geol. Soc. Am. Bull., 100, 948–969, doi:10.1130/0016-
895 7606(1988)100<0948:TFPTAL>2.3.CO;2, 1988.
896 Hemmingsen, E.: Permeation of gases through ice, Tellus, 11, 355–359, doi:10.1111/j.2153-
897 3490.1959.tb00041.x, 1958.
898 Holocher, J., Peeters, F., Aeschbach-Hertig, W., Kinzelbach, W., and Kipfer, R.: Kinetic model
899 of gas bubble dissolution in groundwater and its implications for the dissolved gas composition,
900 Environ. Sci. and Technol., 37, 1337–1343, doi:10.1021/es025712z, 2003.

901 Huttunen, J. T., Alm, J., Liikanen, A. Juutinen, S., Larmola, T., Hammar, T., Silvola, J., and
902 Martikainen, P. J.: Fluxes of methane, carbon dioxide and nitrous oxide in boreal lakes and
903 potential anthropogenic effects on the aquatic greenhouse gas emissions, Chemosphere, 52, 609–
904 621, doi:10.1016/S0045-6535(03)00243-1, 2003.
905 Intergovernmental Panel on Climate Change (IPCC): Climate Change 2013: The Physical
906 Science Basis, Cambridge University Press, Cambridge, United Kingdom and New York, USA,
907 1535 pp., 2013.
908 Jakkila, J., Leppäranta, M., Kawamura, T., Shirasawa, K., and Salonen, K.: Radiation transfer
909 and heat budget during the ice season in Lake Pääjärvi, Finland, Aquat. Ecol., 43, 681–692,
910 doi:10.1007/s10452-009-9275-2, 2009.
911 Kanevskiy, M., Shur, Y., Fortier, D., Jorgenson, M. T., and Stephani, E.: Cryostratigraphy of late
912 Pleistocene syngenetic permafrost (yedoma) in northern Alaska, Itkillik River exposure,
913 Quaternary Res., 75, 584–596, doi:10.1016/j.yqres.2010.12.003, 2011.
914 Kankaala, P., Taipale, S., Nykänen, H., and Jones, R. I.: Oxidation, efflux, and isotopic
915 fractionation of methane during autumnal turnover in a polyhumic, boreal lake, J. Geophys. Res.,
916 112, G02003, doi:10.1029/2006JG000336, 2007.
917 Keller, M. and Stallard, R. F.: Methane emission by bubbling from Gatun Lake, Panama, J.
918 Geophys. Res., 99, 8307–8319, doi:10.1029/92JD02170, 1994.
919 Kelly, C. A. and Chynoweth, D. P.: The contributions of temperature and the input of organic
920 matter in controlling rates of sediment methanogenesis, Limnol. Oceanogr., 26, 891–897, 1981.
921 Kessler, M. A., Plug, L., and Walter Anthony, K.: Simulating the decadal to millennial scale
922 dynamics of morphology and sequestered carbon mobilization of two thermokarst lakes in NW
923 Alaska, J. Geophys. Res., 117, doi:10.1029/2011JG001796, 2012.

924 Kling, G. W., Kipphut, G. W., and Miller, M. C.: The flux of CO_2 and CH_4 from lakes and rivers
925 in arctic Alaska, Hydrobiologia, 240, 23–36, doi:10.1007/BF00013449, 1992.
926 Lidstrom, M. E. and Somers, L.: Seasonal study of methane oxidation in Lake Washington,
927 Appl. Environ. Microb., 47, 1255–1260, 1984.
928 Liikanen, A., Huttunen, J. T., Valli, K., and Martikainen, P. J: Methane cycling in the sediment
929 and water column of mid-boreal hyper-eutrophic Lake Kevaton, Finland, Arch. Hydrobiol., 154,
930 585–603, 2002.
931 Liston, G. E. and Sturm, M.: Winter precipitation patterns in arctic Alaska determined from a
932 blowing snow model and snow-depth observations, J. Hydrometeorol., 3, 646–659,
933 doi:10.1175/1525-7541(2002)003<0646:WPPIAA>2.0.CO;2, 2002.
934 Lofton, D. D., Whalen, S. C., and Hershey, A. E.: Effect of temperature on methane dynamics
935 and evaluation of methane oxidation kinetics in shallow Arctic Alaskan lakes, Hydrobiologia,
936 721, 209–222, doi:10.1007/s10750-013-1663-x, 2014.
937 Mackay, J. R.: Disturbances to the tundra and forest tundra environment of the western Arctic,
938 Can. Geotech. J., 7, 420–432, doi:10.1139/t70-054, 1970.
939 Martinez-Cruz, K., Sepulveda-Jauregui, A., Walter Anthony, K. M., and Thalasso, F.:
940 Latitudinal and seasonal variation of aerobic methane oxidation in Alaskan lakes,
941 Biogeosciences, in preparation, 2014.
942 Mattson, M. D. and Likens, G. E.: Air pressure and methane fluxes, Nature, 347, 718–719,
943 doi:10.1038/347718b0, 1990.
944 Michmerhuizen, C. M., Striegl, R. G., and McDonald, M. E.: Potential methane emission from
945 north-temperate lakes following ice melt, Limnol. Oceanogr., 41, 985–991, 1996.

946 Muhs, D. R. and Budahn, J. R.: Geochemical evidence for the origin of late Quaternary loess in
947 central Alaska, Can. J. Earth Sci., 43, 323–337, doi:10.1139/e05-115, 2006.
948 Nye, J. F.: The geometry of water veins and nodes in polycrystalline ice, J. Glaciol., 35, 17–22,
949 doi:10.3189/002214389793701437, 1989.
950 Péwé, T. L.: Quaternary geology of Alaska, United States Geological Survey Professional Paper
951 835, United States Government Printing Office, Washington, D. C., USA, 145 pp., 1975.
952 Phelps, A. R., Peterson, K. M., and Jeffries, M. O.: Methane efflux from high-latitude lakes
953 during spring ice melt, J. Geophys. Res., 103, 29029–29036, doi:10.1029/98JD00044, 1998.
954 Reyes, A. V., Froese, D. G., and Jensen, B. J. L.: Permafrost response to last interglacial
955 warming: Field evidence from non-glaciated Yukon and Alaska, Quaternary Sci. Rev., 29, 3256-
956 3274, doi:10.1016/j.quascirev.2010.07.013, 2010.
957 Rudd, J. W. M. and Hamilton, R. D.: Methane cycling in a eutrophic shield lake and its effects
958 on whole lake metabolism, Limnol. Oceanogr., 23, 337–348, doi:10.4319/lo.1978.23.2.0337,
959 1978.
960 Sasaki, M., Imura, S., Kudoh, S. Yamanouchi, T., Morimoto, S., Hashida, G.: Methane efflux
961 from bubbles suspended in ice-covered lakes in Syowa Oasis, East Antarctica, J. Geophys. Res.,
962 114, D18114, doi:10.1029/2009JD011849, 2009.
963 Schulz, S., Matsuyama, H., Conrad, R.: Temperature dependence of methane production from
964 different precursors in a profundal sediment (Lake Constance), FEMS Microbiol. Ecol., 22, 207–
965 213, doi:10.1111/j.1574-6941.1997.tb00372.x, 1997.
966 Sepulveda-Jauregui, A., Hoyos-Santillan, J., Martinez-Cruz, K., Belmonte-Izquierdo, Y., Walter
967 Anthony, K. M., Casper, P., and Thalasso, F.: Eutrophication exacerbates potential methane

968 production and consumption response in lake ecosystems to warming, Environ. Sci. Technol., in
969 preparation, 2014a.
970 Sepulveda-Jauregui, A., Walter Anthony, K. M., Martinez-Cruz, K., Greene, S., and Thalasso,
971 F.: Methane and carbon dioxide emissions from 42 lakes along a North-South latitudinal transect
972 in Alaska, Biogeosciences, in preparation, 2014b.
973 Smith, L. K. and Lewis Jr., W. M.: Seasonality of methane emissions from five lakes and
974 associated wetlands of the Colorado Rockies, Global Biogeochem. Cy., 6, 323–338,
975 doi:10.1029/92GB02016, 1992.
976 Stepanenko, V. M., Machul'skaya, E. E., Glagolev, M. V., and Lykossov, V. N.: Numerical
977 modeling of methane emissions from lakes in the permafrost zone, Izv. Atmos. Ocean. Phys., 47,
978 252–264, doi:10.1134/S0001433811020113, 2011.
979 Sturm, M., Holmgren, J., König, M., and Morris, K.: The thermal conductivity of seasonal snow,
980 J. Glaciol., 43, 26–41, 1997.
981 Tang, K. M., McGinnis, D. F., Frindte, K., Brüchert, V., and Grossart, H.-P.: Paradox
982 reconsidered: Methane oversaturation in well-oxygenated lake waters, Limnol. Oceanogr., 59,
983 275–284, doi:10.4319/lo.2014.59.1.0275, 2014.
984 Van Bodegom, P., Goudriaan J., and Leffelaar P.: A mechanistic model on methane oxidation in
985 a rice rhizosphere, Biogeochemistry, 55, 145–177, doi:10.1023/A:1010640515283, 2001.
986 Walter Anthony, K. M. and Anthony, P.: Constraining spatial variability of methane ebullition
987 seeps in thermokarst lakes using point process models, J. Geophys. Res., 118, 1–20,
988 doi:10.1002/jgrg.20087, 2013.

989 Walter Anthony, K. M., Vas, D. A., Brosius, L., Chapin III, F. S., Zimov, S. A., and Zhuang, Q:
990 Estimating bubble emissions from northern lakes using ice-bubble surveys, Limnol. Oceanogr.
991 Meth., 8, 592–609, 2010.
992 Walter, K. M., Chanton, J. P., Chapin III, F. S., Schuur, E. A. G., and Zimov, S. A.: Methane
993 production and bubble emissions from arctic lakes: Isotopic implications for source pathways
994 and ages, J. Geophys. Res., 113, G00A08, doi:10.1029/2007JG000569, 2008.
995 Walter, K. M., Zimov, S. A., Chanton, J. P., Verbyla, D., and Chapin III, F. S.: Methane
996 bubbling from Siberian thaw lakes as a positive feedback to climate warming, Nature, 443, 71–
997 75, doi:10.1038/nature05040, 2006.
998 Wania, R., Ross, I., and Prentice, I. C.: Implementation and evaluation of a new methane model
999 within a dynamic global vegetation model: LPJ-WHyMe v1.3.1, Geosci. Model Dev., 3, 565–
1000 584, doi:10.5194/gmd-3-565-2010, 2010.
1001 Whalen, S. C.: Biogeochemistry of methane exchange between natural wetlands and the
1002 atmosphere, Environ. Eng. Sci., 22, 73–94, doi:10.1089/ees.2005.22.73, 2005.
1003 Wilhelm, E., Battino, R., and Wilcock, R. J.: Low-pressure solubility of gases in liquid water,
1004 Chem. Rev., 77, 219–262, doi:10.1021/cr60306a003, 1977.
1005 Williams, G. P.: Water temperature during the melting of lake ice, Water Resour. Res., 5, 1134–
1006 1138, doi:10.1029/WR005i005p01134, 1969.
1007 Woolf, D. K. and Thorpe, S. A.: Bubbles and the air-sea exchange of gases in near-saturation
1008 conditions, J. Mar. Res., 49, 435–466, doi:10.1357/002224091784995765, 1991.
1009 Yamamoto, S., Alcauskas, J. B., and Crozier, T. E.: Solubility of methane in distilled water and
1010 seawater, J. Chem. Eng. Data, 21, 78–80, doi:10.1021/je60068a029, 1976.

1011 Zimov, S. A., Voropaev, Y. V., Davydov, S. P., Zimova, G. M., Davydova, A. I., Chapin III, F.
1012 S., Chapin, M. C.: Flux of methane from north Siberian aquatic systems: Influence on
1013 atmospheric methane, in: Permafrost Response on Economic Development, Environmental
1014 Security and Natural Resources, NATO Science Series 2, 76, Paepe, R. and Melnikov, V. P.
1015 (Eds.), Kluwer Academic Publishers, Dordrecht, Netherlands; Boston, Massachusetts, USA,
1016 511–524, 2001.
1017

Tables

Table 1. Names of the versions of the model discussed as sensitivity analyses in Sects. 3.4 and 3.5 and Appendix A, and descriptions of how they differ from the "Baseline" version, described in Sect. 2.3. At right, the fraction of the total amount of CH_4 in each version released annually from the sediments of Goldstream Lake by diffusion and ebullition that is emitted to the atmosphere without being consumed by methanotrophy.

Version Name	Difference from Baseline	Fraction of CH_4 Emitted to the Atmosphere
Baseline	-	82%
Less Diffusion	Diffusion rate from lake bottom sediments is 5 times less than in "Baseline."	86%
More/Less Black Ice	Snow density is held constant at 300 kg m^{-3}/100 kg m^{-3}.	81%/84%
Greater/Lesser δ_{eff}	δ_{eff} set to 0.15 mm/0.35 mm in the bubble dissolution component.	83%/81%
Episodic Ebullition	Measured ebullition rates from individual seeps are applied to seeps in the model instead of time-smoothed rates (Sect. 2.2.6).	83%
Early/Late Release	All bubbles trapped at A, B, and C seep sites are released on the first/last day of the spring ice-melt period in the model instead of throughout.	81%/85%
Warmer Climate	Air temperatures are increased uniformly by 5 ˚C.	85%

Figures

Figure 1. (a) Photograph showing CH_4-rich bubbles trapped by ice at Goldstream L. in mid-October 2007. (b) Photographs of representative A-, B-, C-, and Hotspot-type seep sites as seen from above in early-winter lake ice. Note the open water at the Hotspot seep site. The black and red markings on the rulers shown are 10 cm apart. (c) Side-view photographs of blocks of ice harvested from above seep sites in spring. Note the hollow cavity in the block harvested from above the Hotspot seep site (at right).

Figure 2. Map of Goldstream Lake showing the location of the LI-7700 Open Path Methane Analyzer used to measure atmospheric CH_4 concentrations, locations of depth measurements, 0.5 m bathymetric isolines, shoreline locations in 2012 and l950, and the thermokarst zone, characterized by eastward thermokarst expansion and high ebullition activity.

Figure 3. Time-smoothed daily ebullition rates, and rates for individually measured seeps as applied in the model, for A-, B-, C-, and Hotspot-type seeps (panels a, b, c, d). Note the difference in scales on Y-axes, including the log scale in panels c and d.

Figure 4. Modeled and measured volume and CH_4 mole fraction of gas inside ice-bubble mesocosm chambers in the spring 2011 (a) and fall 2011 (b) trials. Values of $\delta_{eff} = 0.25$ mm and 0.27 mm were found to give the best fits to volume and composition measurements for the spring and fall trials, respectively. Values of $\delta_{eff} = 0.35$ mm and 0.15 mm encompassed the range of uncertainty in these measurements, so they were used in sensitivity analyses (Sect. A3).

Figure 5. Modeled and measured thicknesses of (a) black ice, (b) white ice, (c) lake surface snow, and (d) the ice layer (white and black ice) during the winter of 2011–2012. A value of α = 0.95 was used in the ice growth model (Sect. 2.3.2) for this period.

Figure 6. Modeled and measured total thicknesses of the ice layer (white and black ice) during the winter of 2010–2011. Measurements were obtained in areas where snow was occasionally compacted by foot traffic, an effect accounted for in the modeled thickness. A value of α = 0.94 was used in the ice growth model for this period.

Figure 7. (a) A cross section of the model's representation of trapped gas at A, B, and C seep sites. The dashed line indicates the area over which CH_4 dissolves into the water column. Gas beneath the ice-water interface is modeled as a cylinder with constant height (5.7 mm). The volume and radius of this cylinder decrease (indicated by arrows) as the ice grows downward and CH_4 diffuses out, giving rise to the tapering shape of encapsulated bubbles. (b) Schematic of a closed Hotspot seep site. The cavity's shape is determined by field measurements, and its bottom radius determines that of the cylinder of gas beneath the ice-water interface. The height of this cylinder decreases as CH_4 diffuses out and the ice grows downward (indicated by arrows). Note the different scales in (a) and (b).

Figure 8. The measured amounts of (a) CH_4 and (b) O_2 dissolved in the water column of Goldstream Lake during the study period, and those calculated in the "Baseline" and "Less Diffusion" versions of the model (Sect. A1).

Figure 9. Measured depth profiles of (a, d) temperature, (b, e) dissolved CH_4 concentration, and (c, f) dissolved O_2 concentration in the water column of Goldstream Lake during the summers of 2011 and 2012. 2011 profiles indicate that fall overturn had occurred by 6 October 2011.

Figure 10. Seasonal and annual quantities of CH_4 dissolving into the water column from ebullition seeps and sediments in the "Baseline" version of the model. Annually, 77% of dissolved CH_4 in Goldstream Lake originates from ebullition bubbles trapped beneath winter ice and 23% from CH_4 diffusion from bottom sediments.

Figure 11. (a) Modeled daily CH_4 emissions to the atmosphere by each of the five mechanisms discussed in Sect. 3.2 in the "Baseline" version of the model. Percentages in the legend denote the fraction of total annual emissions from each emissions mode. (b) Measured atmospheric CH_4 concentrations over Goldstream Lake shown with modeled emissions during a portion of the study period. 2011 ice-off occurred on 15 May, after the period shown.

Figure 12. The fates of seep ebullition bubbles (a) and dissolved CH_4 (b) during the 2-year study period, as calculated in the "Baseline" version of the model. The names of the various modes of CH_4 emission are discussed in Sect. 3.2.

Figure 13. The shapes of bubbles encapsulated by lake ice above an A-type ebullition seep. Field measurements of bubbles (a) and (b) are compared to shapes calculated in the bubble dissolution component of the model (Sect. 2.3.3). Plots represent a side profile of bubbles, with the y-axis representing depth within the ice layer. Note the different scales on both axes. (c) Encapsulated

bubbles oriented in both directions, either with flat bottoms and tapering tops, or vice-versa. Photos courtesy of Melanie Engram.

Figures

a)

b)

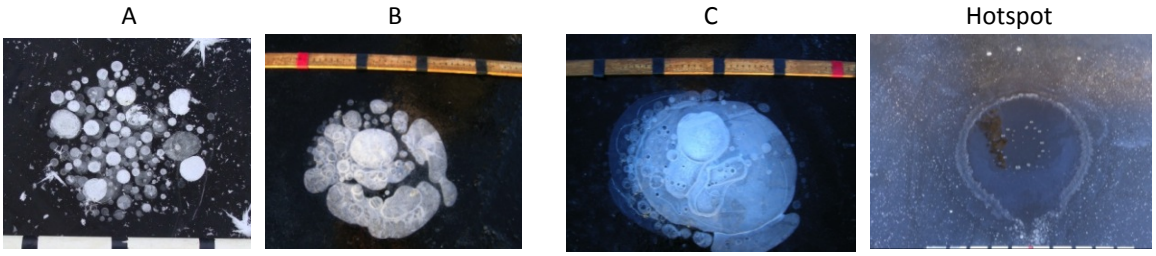

c)

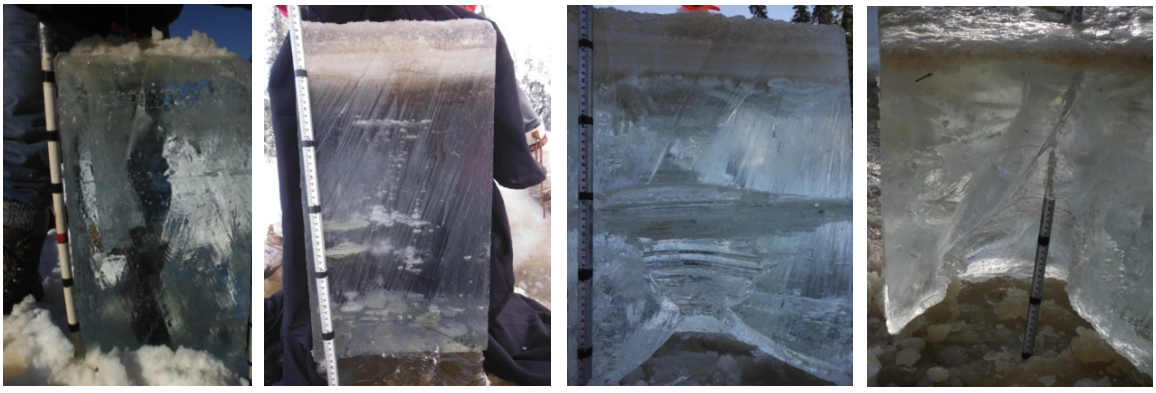

Figure 1

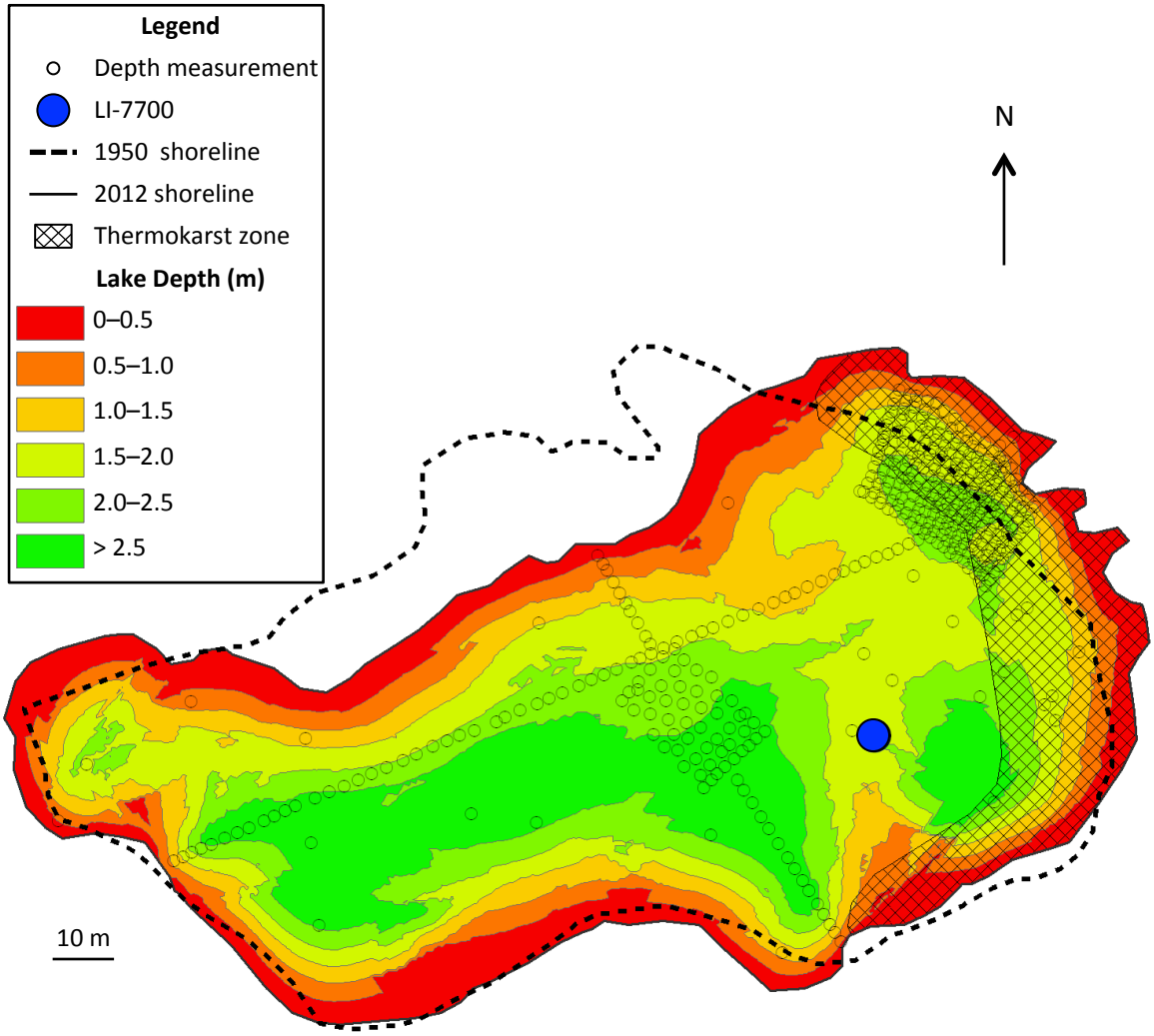

1104

1105 **Figure 2**

1106

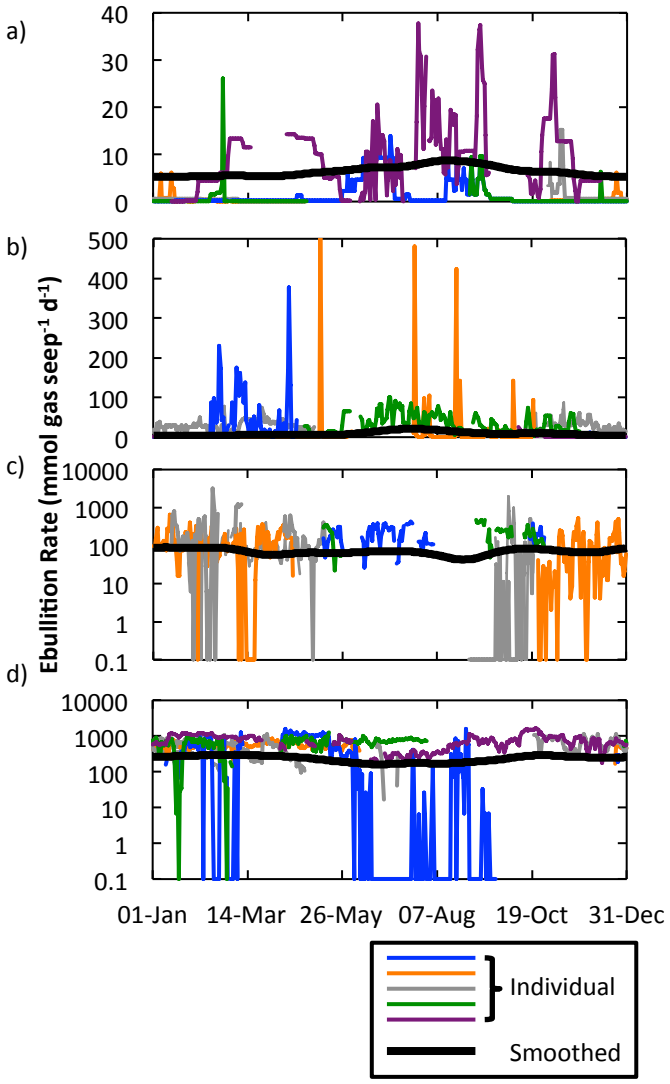

1107

1108 **Figure 3**

1109

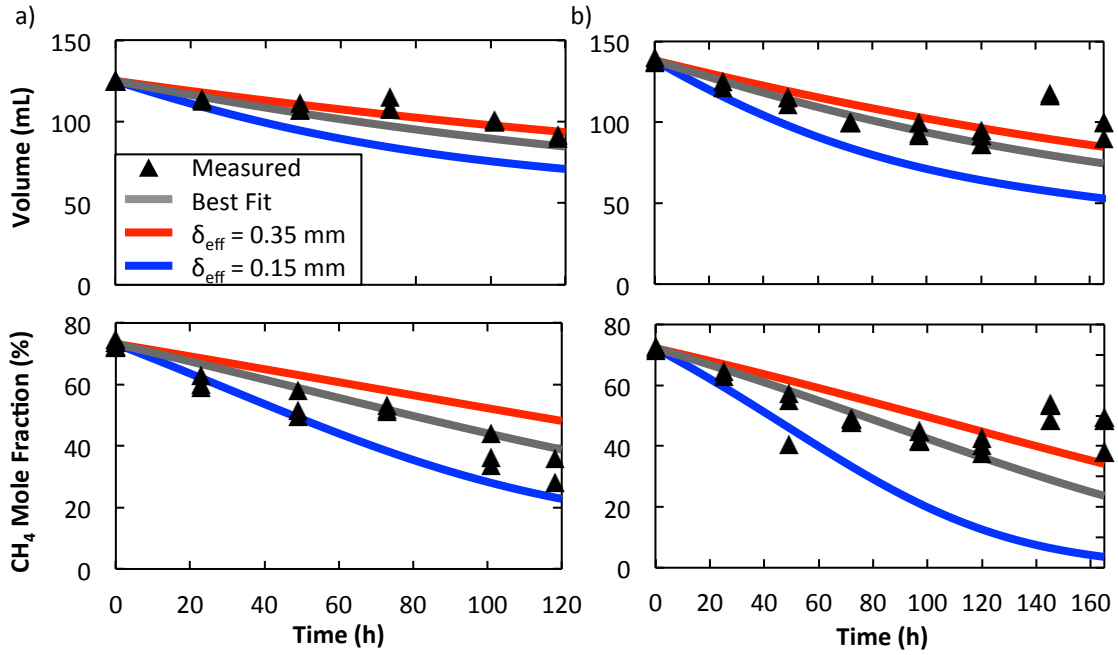

1110

1111 **Figure 4**

1112

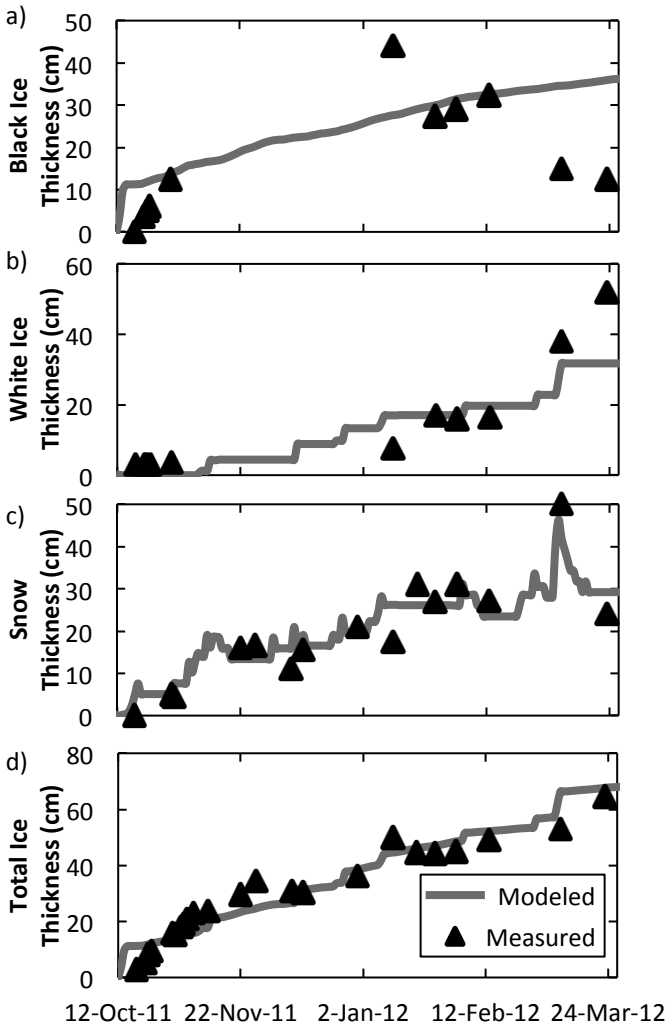

1113

1114 **Figure 5**

1115

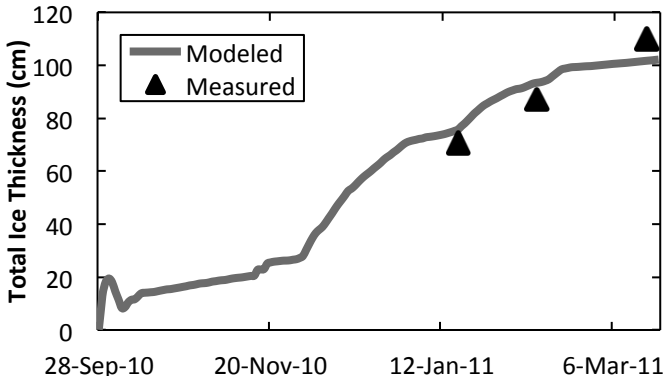

1116

1117 **Figure 6**

1118

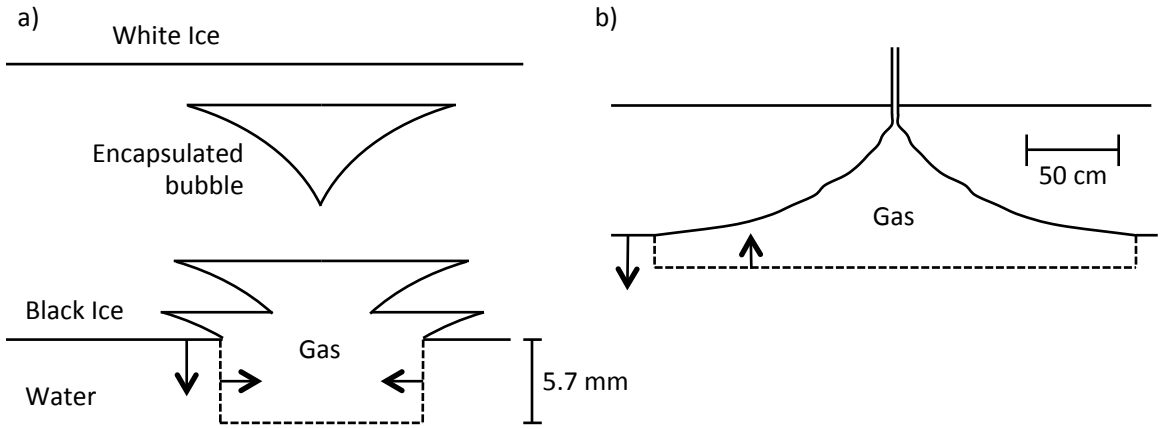

1119

1120 **Figure 7**

1121

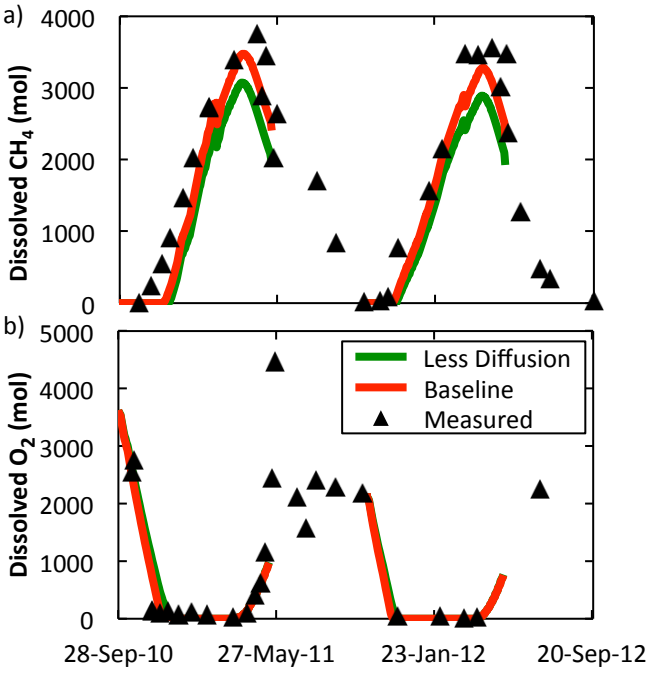

1122

1123 **Figure 8**

1124

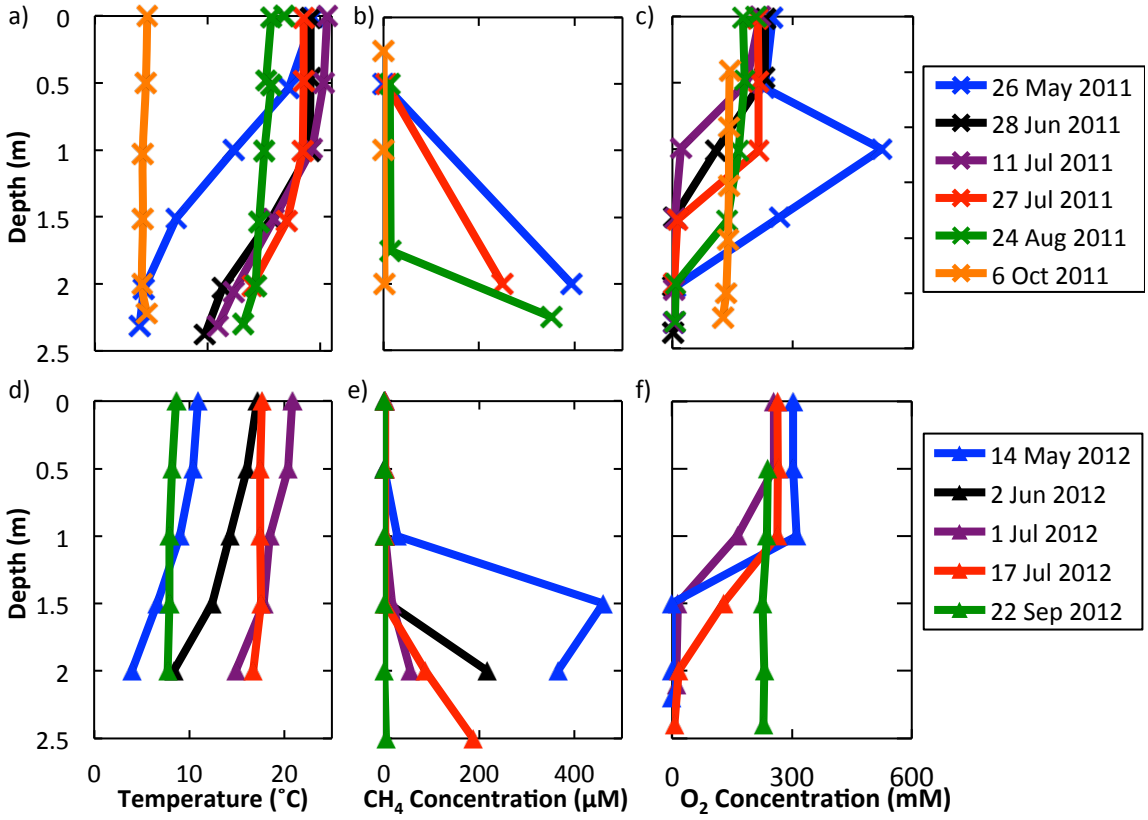

1125

1126 **Figure 9**

1127

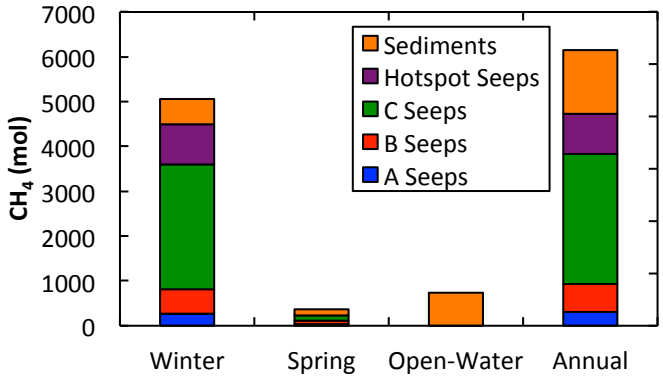

1128

1129 **Figure 10**

1130

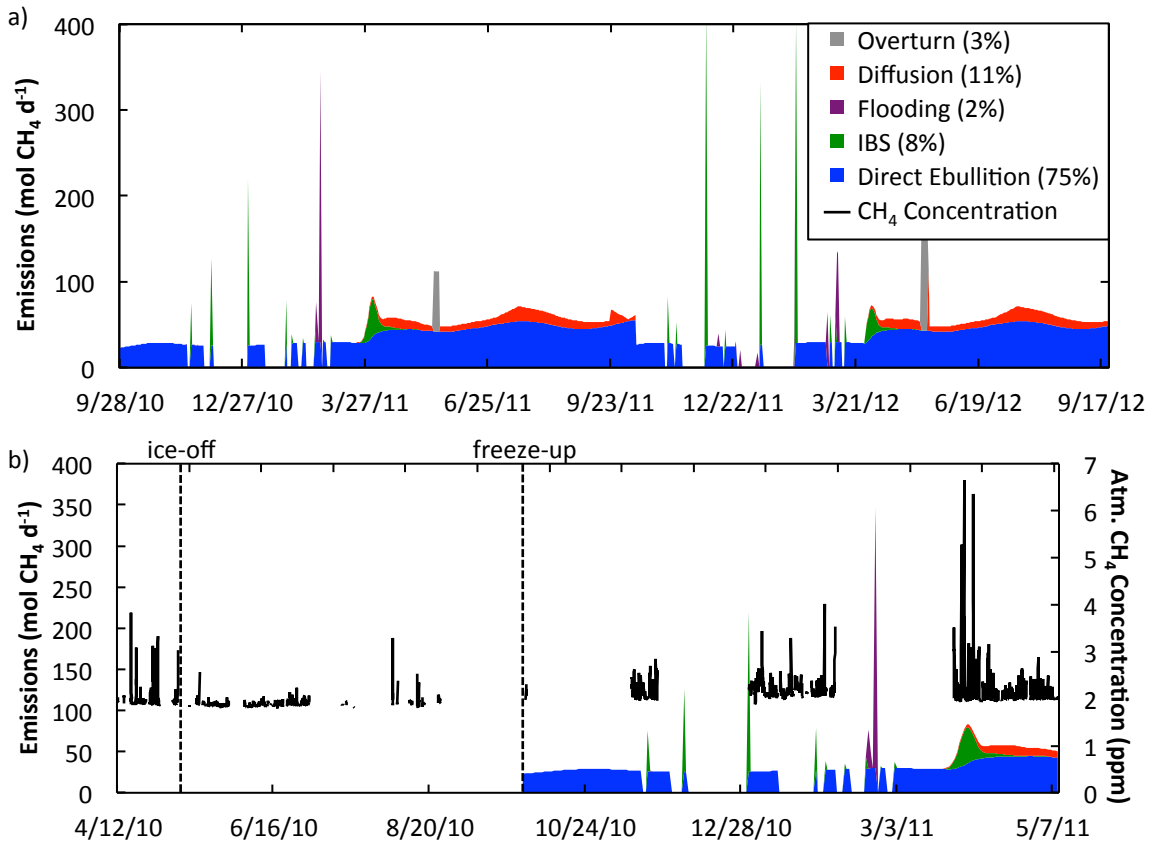

1131

1132 **Figure 11**

1133

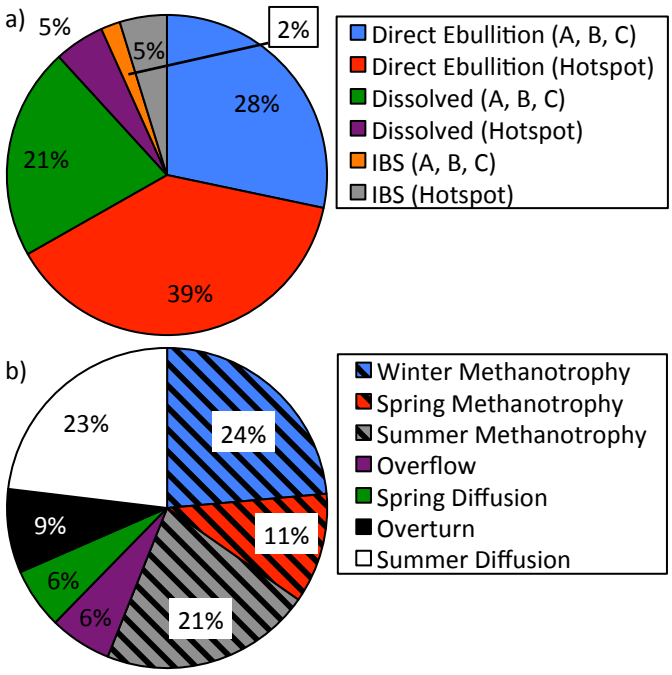

1134

1135 **Figure 12**

1136

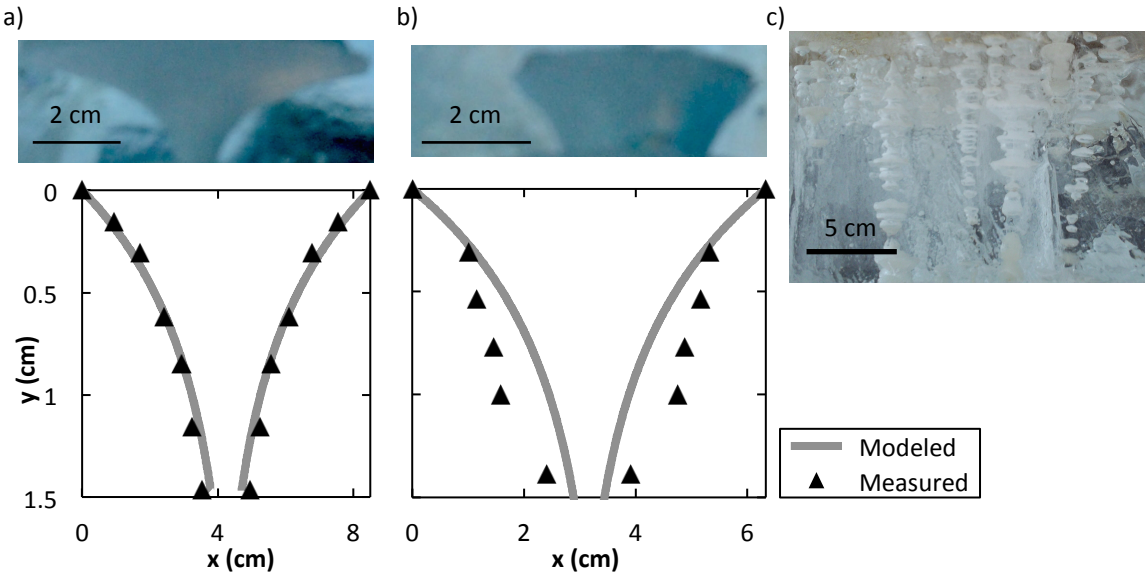

1137

1138 **Figure 13**

1139